Article

Site Effect Potential in Fond Parisien, in the East of Port-au-Prince, Haiti

Sophia Ulysse [1,2,3], Dominique Boisson [1], Valmy Dorival [1,2,3], Kelly Guerrier [1], Claude Préptit [2], Léna Cauchie [3], Anne-Sophie Mreyen [3] and Hans-Balder Havenith [3,*]

1   Unité de Recherche en Géosciences, Faculté des Sciences, Université d'Etat d'Haiti, 10 Impasse Ambroise, Port-au-Prince, Haiti; sophiaulysse@gmail.com (S.U.); dominique.boisson@ueh.edu.ht (D.B.); valmy.dorival@ueh.edu.ht (V.D.); kelly.guerrier@ueh.edu.ht (K.G.)
2   Unité Technique de Sismologie, Bureau des Mines et de l'Energie, Delmas 31, Port-au-Prince, Haiti; claudeprepetit@hotmail.com
3   Department of Geology, University of Liege, Place du 20-Août, 7B- 4000 Liège, Belgium; lena.cauchie@uliege.be (L.C.); as.mreyen@uliege.be (A.-S.M.)
*   Correspondence: HB.Havenith@uliege.be

Abstract: In the frame of a Belgo-Haitian cooperation project (PIC 2012–2016), a study of the local seismic hazard was performed in Fond Parisien, an area located on the foothills of the "Massif de la Selle", along the easternmost portion of the Enriquillo Plantain Garden Fault (EPGF). The H/V Spectral Ratio (HVSR) technique was applied to study the resonance frequency of the target areas and the azimuth of the wave field. The amplification factors were estimated using Standard Spectral Ratios obtained from earthquakes recorded by a temporary seismic network. Using the Multichannel Analysis of Surface Waves method, the seismic properties of the shallow layers were investigated. Then, the results were compared to local Electrical Resistivity Tomography data. These results highlight, in the central part of Fond Parisien, an E-W zone of low velocities ranging from 200 m/s to 450 m/s and low resistivities between 1 Ωm and 150 Ωm, due both to tectonic folding of the rocks and to the presence of sediment filling in the eastern part. The latter is marked, in most of its sites, by resonances at one or more frequencies ranging from 0.7 Hz to 20 Hz. Infiltration and storage of brackish water in the underground layers also contribute to the low resistivity values. With the noise HVSR data, we also evidenced a significant influence of the EPGF on the main orientation of the seismic wavefield as in the vicinity of this fault, the azimuths are parallel to the orientation of the fault. Overall, the results also show greater potential for site effects in the block formed by the sedimentary basin and strong amplification of the seismic ground motion for the sites bordering the basin to the north and west. We interpret the amplification in the north and south-west as probably originating from topographic irregularities locally coupled with sediment deposits, while in the center of the western part, the site effects could be explained by the presence of folds and related weakened and softened rocks. By the integration of several geophysical methods, we could distinguish areas where it is possible to build more safely. These zones are located in the northern part and encompass Quisqueya Park and neighboring areas as well as the village "La Source" in the southern part. In the rest of Fond Parisien, i.e., in the more central and eastern parts, buildings should be erected with caution, taking into account the nearby presence of the EPGF and the influence of fine sediments on the amplification of the seismic motion.

Keywords: applied geophysics; soft soils; site effect distribution maps; EPGF; Haiti

1. Introduction

The Haiti earthquake, which occurred on 12 January 2010, was a very catastrophic event. In terms of human losses, it ranks among the five most disastrous earthquake events in history [1]; considering the affected part of the country and related population hit by the disaster, it could even be classified as the worldwide largest historical natural disaster at

country-scale [1]. One can therefore wonder about the causes of such a catastrophe that was induced by a non-exceptionally large earthquake. The question has been analyzed from several perspectives. The first criteria highlighted was the location of the epicentre near a densely populated area, according to United States Geological Survey (USGS), at 27 km WSW of Port-au-Prince. Second, the high vulnerability of the population with respect to earthquake hazards (according to Bilham [2]) and the related lack of risk awareness and preparedness have been put forward as elements contributing to the extreme impacts [3]. Yet, Haiti had already been hit by several catastrophic events in the past. The 9 November 1701, as well as the 21 and 22 November 1751 earthquakes (see location in Figure 1), are, among others, events that ravaged Port-au-Prince and its surroundings [4]. Some of them were felt in almost all over the country and are also thought to have ruptured the Enriquillo Plantain Garden Fault (EPGF) [5].

After the January 2010 earthquake, a series of papers analysed the seismological and engineering aspects of the event and examined statistics of building damage with respect to geologic, geotechnical and topographical soil profiles. Regional hazard estimates were first revised by Frankel et al. [6] who proposed a new probabilistic seismic hazard map for the country. Based on the available information on fault slip rates for major crustal faults, subduction zones and historical as well as instrumental seismicity, these maps provide firm-rock peak ground acceleration values (Figure 1a) and a grid of shallow shear-wave velocities estimated from topographic slope [6]. New seismic hazard maps were proposed by Frankel et al. [7], as more data became available, these latter maps show a peak ground acceleration of 0.25 g–0.3 g for Port-au-Prince. McNamara et al. [8] worked on the computation of attenuation laws for Hispaniola Island. Cox et al. [9] proposed a seismic site classification microzonation for Port-au-Prince based on shear wave velocity V_S profiles collected throughout the city. A microzonation study has also been performed by Terrier and Bialkowski [10]. With regard to site effect, the city of Port-au-Prince and some of its neighboring areas have been studied by several groups among which Hough et al. [11], Assimaki and Jeong [12] and St Fleur et al. [13]. More recently, Ulysse et al. [14,15], by integrating several investigation and modelling methods, provided small-scale distribution maps of the site effects throughout a hilly area located in the Southeast of Port-au-Prince. Overall of these studies were especially focused on the central part of the EPGF.

Now we present the results of a detailed study of local seismic hazard for an area that is located near the EPGF, but in the easternmost part of Haiti, Fond Parisien (investigated zone outlined in Figure 1b). Our work integrates geophysical, geotechnical and seismological data that were obtained from numerous H/V Spectral Ration (HVSR) measurements, Electrical Resistivity sections, Seismic tests, and a small temporary seismic network in this area to better constrain the sub-regional seismic microzonation.
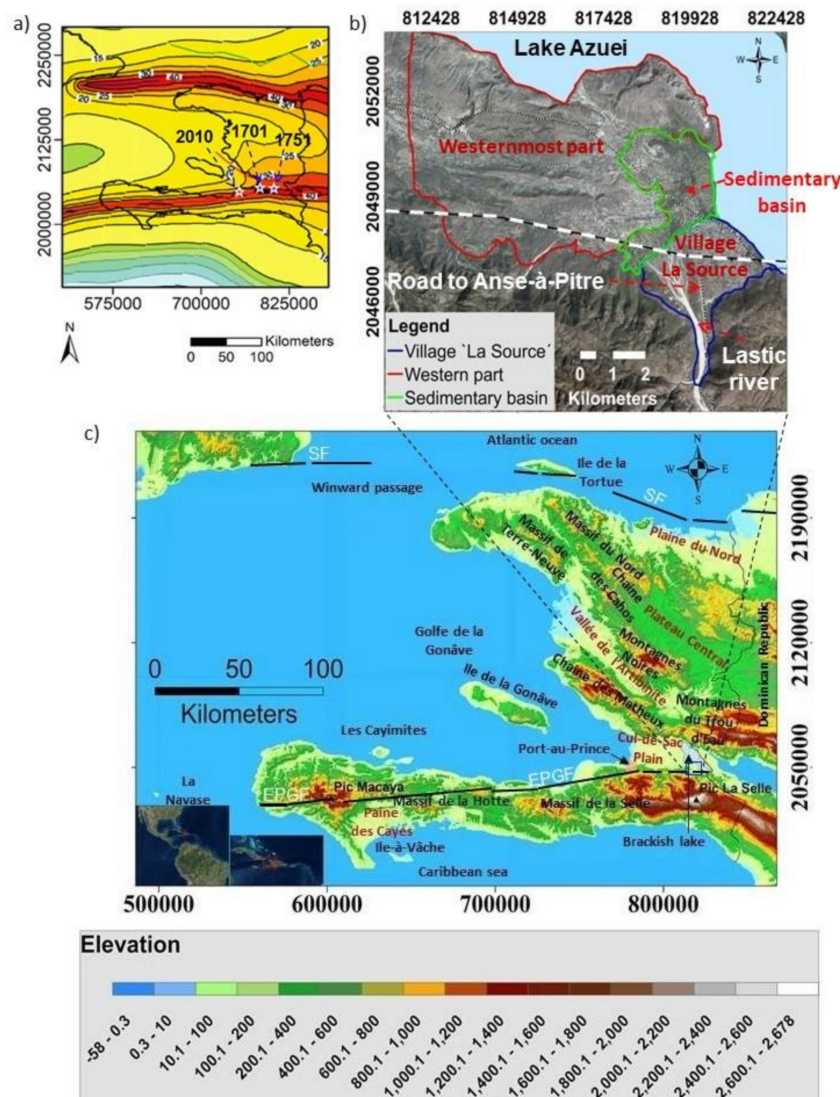
Figure 1. (**a**) Seismic hazard map for Haiti with 10% exceedance probability in 50 years. Large historical earthquakes and higher peak ground acceleration are located on/near Enriquillo Plantain Garden Fault (EPGF) and Septentrional Fault (SF). (**b**) The Fond Parisien area with the village "La Source" outlined in blue and the Cul-de-Sac plain shown in green; modified from Frankel et al. [7]. (**c**) Topographic map of Haiti showing the location of the district of Fond Parisien in Haiti. SF and EPGF are respectively Septentrional Fault Enriquillo Pantain Garden Fault.

2. Fond Parisien: Geographic Context and Geological Setting

The target zone of Fond Parisien is located near the southeastern Haitian–Dominican border, at 37 km to the East of Port-au-Prince, the capital of Haiti. It belongs to the second driest zone of the country and is part of the Cul-de-Sac plain. The latter extends from the Port-au-Prince bay in the West to Lake Azuei in the East. Its altitude regularly increases from the western coastline of the Port-au-Prince bay to Lake Azuei where it reaches 160 m. It is delimited in the North and East by Lake Azuei. In the South, it is bounded by the northern foothills of the "Massif de la Selle". The latter is the highest mountain range of the Republic of Haiti. It extends over a length of about 100 km along its West–East axis and a width of about 32 km. The axis of its main range contains the highest summit of Haiti with an altitude of 2680 m. Its basement consists of a Lower to Upper Cretaceous complex of igneous rocks (basalt and dolerite). The basalt layers constituting the core of the massif are, in some areas, interbedded with Albian–Aptian limestones. The group of Cretaceous rocks is unconformably overlaid by the basal conglomerate of the marine Paleocene–Eocene and

the Oligo–Miocene series consisting of sandstones, claystones, other coarse conglomerates and limestones. These series are covered by the "Formation Morne Delmas" and constitute the last foothills of the "Massif de la Selle", dominating thus the Cul-de-Sac Plain. The latter which is frequently considered as a graben (as by Maurasse [16]) is a synclinorium showing faulted folds with vergence to the north and to the south respectively in its southern and northern borders [17]. This hypothesis is not in agreement with the compressional faults bordering the southern and the northern edge of the Cul-de-Sac plain and is interpreted by Butterlin [18] as being related to a set of normal faults during the Plio-Pléistocène.

The lithology of the area is essentially composed of series dating from Pliocene and Quaternary age. These series, originally marine, are fed by sedimentary deposits coming from the "Massif de la Selle". The geology of the area presents several facies. Succinctly, the southeastern sheet of the 1/250,000 geologic map of Haiti [19] shows some Quaternary series in the eastern part and Pliocene series in the West. These Pliocene western series form terraces and hills overhanging the Cul-de-Sac plain of about 50 m. According to Butterlin [18], these terraces date from Pleistocene and are mostly constituted of consolidated alluvium.

With a surface area of about 100 km^2, the study zone is thus marked by a very diverse morphology encompassing hills, a basin, a lake and an alluvial fan (Figure 1b, the village "La Source" is located on the alluvial fan). Such morphology seems to be controlled by tectonic activities and hydrogeological features. The recent tectonic activity of the area is controlled by the south-dipping oblique-slip extension of the Enriquillo–Plantain Garden Fault and in-echelon folds affecting the Neogene deposits. Indeed, most of the in-situ sediments are affected by low hills indicating a disturbance of the area by active folds. The most significant one is the roughly EW in-echelon Ganthier fold which is subparallel to the EPGF trace. The eastern part of this 1–2 km wide fold constitutes the central zone of the western part of Fond Parisien and includes Pliocene marine marly sediments [20]. This folding activity seems to be in connection with the activity of the south-dipping extension of EPGF. The reverse oblique-slip motion which mostly generates compressional deformation as indicated by Saint-Fleur [20] and Symithe and Calais [21] could give rise to the NW-SE and roughly E-W deformations observed respectively along the northeastern limit of the study area and along the Ganthier fold.

The sedimentary basin is covered by Quaternary fine soft alluvium to the North of the alluvial fan. Its morphology is related to the orogenesis of the island. The Cul-de-Sac—Enriquillo Trough, to which Fond Parisien belongs, was the last submerged land of Hispaniola Island [18]. The contrasting subsidence of the Cul-de-Sac—Enriquillo Trough with respect to the two prominent septentrional and meridional mountainous structures is evidence of this late emergence. The brackish Lake Azuei is, with the Lake Enriquillo, proof of an arm of the sea which could be trapped during the enclosure [18].

The hydrogeological context of the area is dominated by a fractured and porous carbonate aquifer and some scarce rivers, of which the most important one is the river Lastic (Figure 2) [22]. It flows from the northern foothills of the "Massif de la Selle" to the Lake Azuei and gave rise to the formation of the alluvial fan in the southeastern corner of Fond Parisien. This fan appears to include a former eastern part on which the village "La Source" is settled and a younger western part, i.e., the bed of the river, indicating a westward shift of the latter. It is formed by detrital deposits drained by the river Lastic from the "Massif de la Selle" and is composed of coarse quaternary alluvial materials, typically pebble, gravel and sand. Referring to Butterlin [18], this Quaternary alluvium should encase Miocene detrital conglomerates, sands, sandstone and coarse clay of the "Formation Morne Delmas". The southern area of Fond Parisien contains several limestone quarries exploiting material for construction purposes.
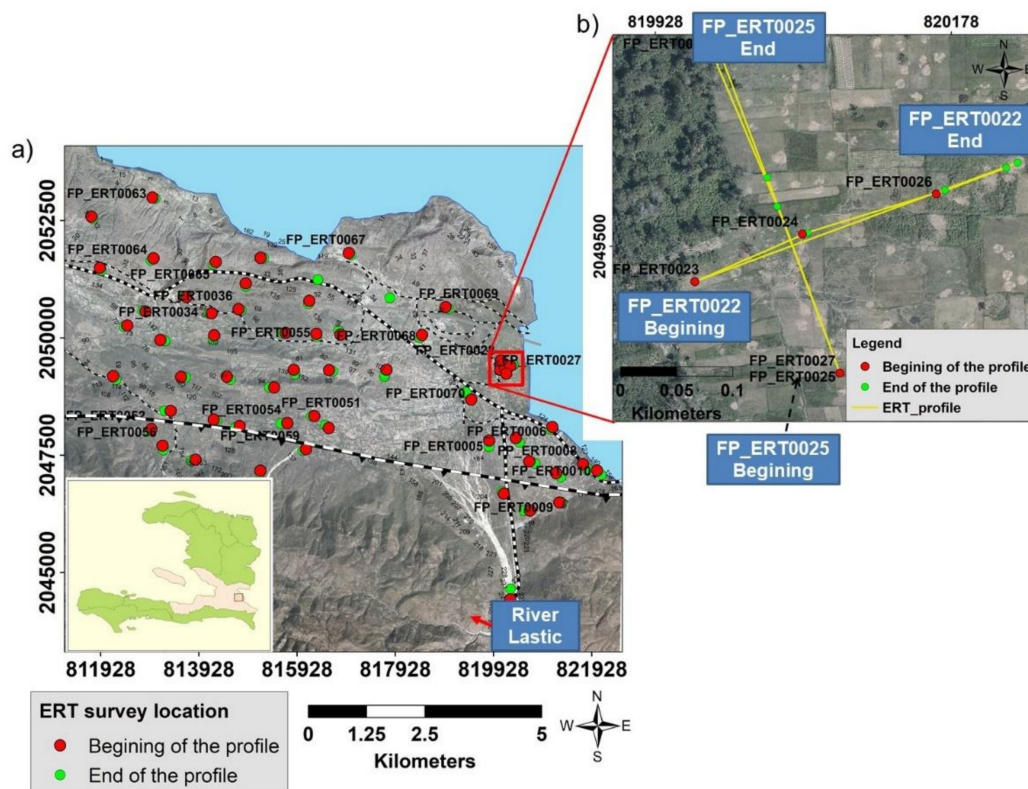
Figure 2. (**a**) Location of the Electrical Resistivity Tomography (ERT) profiles in Fond Parisien, with black roughly E-W trending outline of EPGF (middle part of the map), and the three zones of investigation (La Source village and valley to the South in blue, central sedimentary basin in green and western part, on harder grounds, in red). (**b**) Detailed map of dense ERT measurements on soft soils in the NW of "La Source" village.

3. Geophysical Investigations

Near-surface geophysical methods help determine the electrical and elastic properties of the shallow layers as well as to characterize subsurface structures such as for the identification of faults. The seismological methods can be used to estimate the seismic amplification of the ground, allowing thus to better constrain the site effect distribution. The combined use of electrical, seismic and seismological methods can thus significantly help improve site effect estimates, as for example documented by Giocoli et al. [23] for the High Agri Valley, in Italy.

For the geophysical exploration, Fond Parisien was divided into three areas, on the basis of their morphological characteristics and ground properties. These are: the village "La Source", partly on top of the roughly triangular alluvial cone and southern valley located in the SE corner of the area, the sedimentary basin outlined in green, and the westernmost part marked by the presence of near-surface bedrock in red (see Figure 1b).

3.1. Electrical Resistivity Tomography (ERT) Measurements

ERT surveys are most typically completed in connection with hydrogeological investigations, but have also been widely used to delineate seismic faults [24,25]. This method allows in many cases to establish a relation between the measured resistivity values and the lithological conditions of the subsurface. Nevertheless, the complexity which generally characterizes the subsurface often implies that several factors can contribute to measured outputs and their interpretation may thus not always be straightforward and consequently not unambiguous. Indeed, the same range of resistivity values can be associated to several types of lithology. The advantage of this method is that it is non-invasive whereas one of its greater disadvantages is its difficulty to be used in urbanized sites (as highlighted in the

previous paper, by Ulysse et al. [14] focused on site effect assessment of an urban site in Port-au-Prince).

In the present case, with applications in a more rural context of Fond Parisien, 61 ERT profiles with length varying from 62 to 315 m could be completed all over the target area (see Figure 2). For the measurements, we used a Terrameter SAS 4000 instrument combined with a multi-electrode (64 electrodes with maximal 5 m spacing) acquisition system (ABEM Lund). The two longest ERT profiles were performed in the sedimentary basin next to the lake, i.e., FP_ERT0022 and FP_ERT0025 which respectively measure 315 and 300 m in length. The application of this survey assumes that there are no resistivity variations in directions that differ from the profile orientation; we tested this hypothesis by arranging a nearly perpendicular intersection of these two longest profiles (see detailed map in the right part of Figure 2).

3.2. Seismic Surveys

For the seismic surveys, we exclusively used the acquisition of surface waves. The surface wave methods analyze the geometrical dispersion of surface waves in vertically heterogeneous media (typically marked by increasing shear wave velocities with depth). We applied the Multichannel Analysis of Surface Waves (MASW), which started to be developed by Park et al. [26]. Discussions about the different surface wave methods and their effectiveness can be found in Foti et al. [27], Strobbia [28], Renalier [29], Mucciarelli et al. [30] and Bonnefoy-Claudet et al. [31]. Results are typically represented by a graph called "dispersion curve" that shows the change of surface wave velocities (very close to shear, S-wave, velocities) in the frequency domain. The inversion of the dispersion curve allows us to infer the seismic properties of the subsurface and to obtain the shear wave velocity model of the shallow subsurface [28]. The surface wave methods can be used to estimate the thickness of shallow soft layers, the depth of harder bedrock as well as the degree of fracturing of rocks.

Seismic profiles for 1D MASW analysis were completed in 83 places (green circles on the map in Figure 3a). The length of the profiles, made of 12 vertical geophones of 4.5 Hz, ranged from 22 m (2 m spacing—see example in the lower photograph in Figure 3c) to 55 m (5 m spacing). Shots with a 10 kg sledgehammer were completed at offsets of 4 m to 10 m. Triggered seismic waves were recorded with a DAQLink instrument.
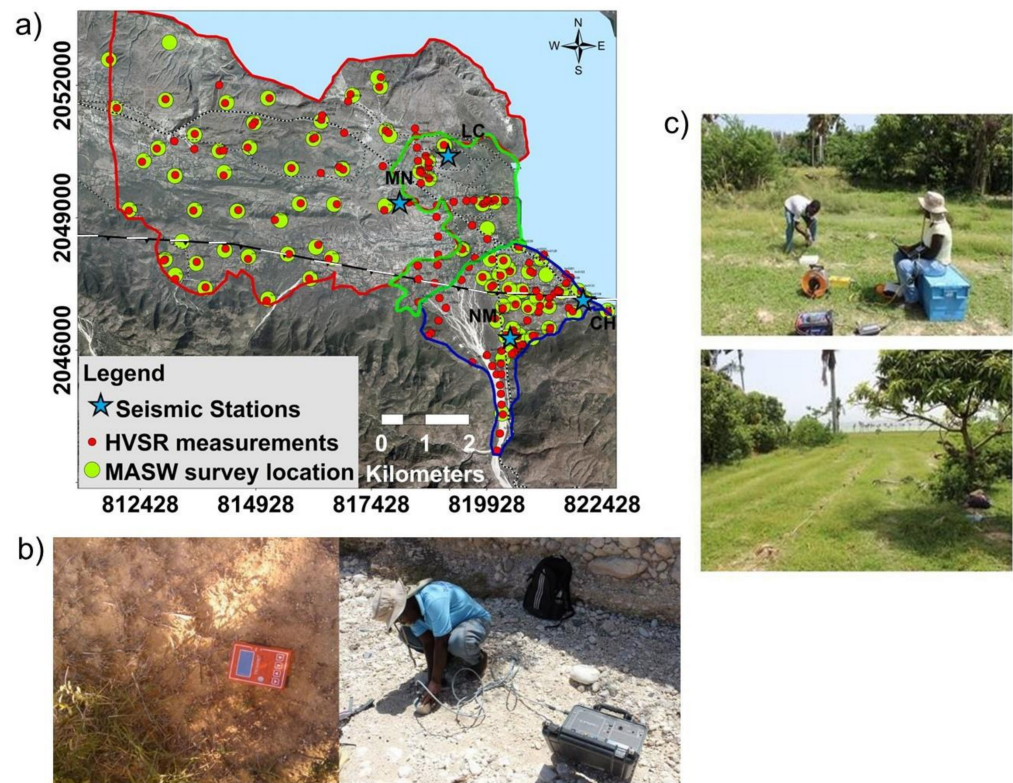
Figure 3. (**a**) Location of the HVSR measurements (red points), seismic stations (blue stars) and seismic profiles (for Multichannel Analysis of Surface Waves (MASW), analysis, light green circles) in Fond Parisien, with outline of EPGF (middle part of the map). (**b**) Photographs of ambient noise TROMINO (left) and CityShark recorders (right, with Lennartz 1Hz seismometer) and installation. (**c**) Photographs of seismic profile and seismic source (hammer impact).

3.3. HVSR Measurements

Commonly referred to as Horizontal to Vertical Spectral Ratio (HVSR) or H/V, the single station test, together with the surface wave seismic methods, is one of the commonly used techniques in the field of seismological site investigation. The H/V technique consists of computing the spectral ratio between the mean of the horizontal components and the vertical component recorded by a single seismic station [32–34]. This technique introduced by Nogoshi and Igarashi [35] became popular after the publication of Nakamura [32] and then reviewed by the European SESAME project [36]. If applied to earthquake data, the method is usually called Earthquake HVSR. Thanks to its simplicity, it is now one of the most commonly used techniques to provide a first estimate of site effects, especially in urban areas. In the case of a one-dimensional medium including a soft sediment layer overlying a bedrock, it provides a good estimation of the resonance frequency (*fo*) at the target site. However, the meaning of the spectral amplitudes is still subjected to discussion. The knowledge of the fundamental resonance frequency *fo* at the measurement point can be used together with the shear wave velocity Vs to estimate the thickness h of the sedimentary layer where the surface waves propagate using the simple equation: *fo = Vs/(4h)* (cf. Ibs-von Seht and Wohlenberg [37]).

In total, 150 ambient noise H/V measurements were completed in Fond Parisien: 76 in the village "La Source", 41 in the westernmost part and 33 in the sedimentary basin (see red points in Figure 3a). They were collected using a 3-component Tromino single station (model ENGY PLUS, 0.1 Hz natural frequency), working in the frequency range of 0.1–1024 Hz on the three channels. Recordings of 20 to 30 min were acquired with a sampling rate of 128 samples per second (sps). Furthermore, in order to validate the Tromino results, a 1 Hz Lennartz 3-component sensor connected to a Cityshark seismic station was also used in 50

places of Fond Parisien. The Cityshark recordings lasted 20 min with a sampling rate of 200 sps (or Hz). Two photographs of HVSR measurements completed with the Tromino and the Lennartz 1 Hz-Cityshark stations are shown, respectively, in the left and right parts of Figure 3b.

3.4. Earthquake Recordings

The most direct geophysical–seismological approach to estimate the potential of a given site to amplify the seismic ground motion is based on the comparison of the earthquake shaking spectrum recorded at the target site with a second record measured at a reference (hard rock) site, as proposed by Borcherdt [38]. This procedure, also known as Standard Spectral Ratio (SSR) assessment, is now widely applied in various geological contexts, preferentially in seismically very active regions. Examples of such studies can be found in Borcherdt and Gibbs [39], Layadi et al. [40], St Fleur et al. [13], Michel et al. [41] and were also presented by the authors of this study in Ulysse et al. [14] for the Gros–Morne site in Port-au-Prince. It provides a good estimation of the resonance frequency and the peak amplitude of the target site.

From the preceding, it becomes clear that one of the requirements of this technique is the recording of the seismic ground motion at a reference station. This latter has to be free of amplification and should ideally be installed on a rock site. In general, this rock is chosen from geological information or in the field where outcropping bedrock is evident. However, in most cases, it is difficult, or even impossible, to find or to access a rock site as recommended by the method. In such cases, the appropriate procedure is to install this reference station on a site where the depth of the bedrock is estimated to be the lowest. In Fond Parisien, some scarce rocky facies were identified in the southwestern area; however, in that zone, there are only sparse houses, not adequate for the installation of a station, notably due to partial absence of electricity. Assuming that the rock is shallower in the parts that are either nearer to the "Massif de la Selle" or close to the southwest part, we decided to record the ground motion at sites located in these areas. We also installed seismic stations in zones that were of particular interest like the sedimentary basin and the northern alluvial fan. The whole temporary seismic network thus consisted of 4 broadband seismometers positioned within a nearly rectangular array as shown by the distribution of stars on the map in Figure 3a. Earthquake data were recorded for 7 months until August 2014, using Güralp type sensors (CMG-40TD) operating with a natural period of 120 s and with selected sampling rates of 100 and 200 sps. Recording stations were called "CH", "LC", "MN" and "NM". The station "NM" is the closest one to the "Massif de la Selle" and was considered as the most appropriate location for serving as reference station, see Section 4.4.2.

4. Data Processing and Results

4.1. ERT Surveys

ERT profiles of the subsurface were obtained by inverting the resistance data measured along the electrical resistivity sections. The inversion is based on a non-linear least-squares optimization technique and is computed using the RES2DINV software [42]. The software first calculates the apparent resistivity values using a forward modeling subroutine, and then iteratively, tries to adjust the 2D apparent resistivity model with the measured resistivity values.

The computed Electrical Resistivity Tomography (ERT) profiles allowed us to identify large variations of resistivity values in Fond Parisien. Typically, the higher resistivity values were obtained for the alluvial fan and for some areas of the northwestern part of Fond Parisien, near the border of Lake Azuei. However, areas in the sedimentary basin and its elongation to the West, are characterized by very low resistivities (<50 Ωm). An investigation depth of 10 m and more was reached by the short spreads of 62 m in the northwestern zone near the edge of the lake. Here, we will focus on resistivity distributions around the village "La Source", near the alluvial fan, where the profiles of 126 m length

provided information on the ground resistivity down to a depth of 18–22 m. The ERT profiles evidenced ground resistivities of 60 to 400 Ωm in most of the sites, while other zones are marked by moderate resistivities in the range of 100–1000 Ωm. Low resistivity zones (15 to 400 Ωm) are located near the northeastern border of the village (upper right sections of Figure 4), along the lake.
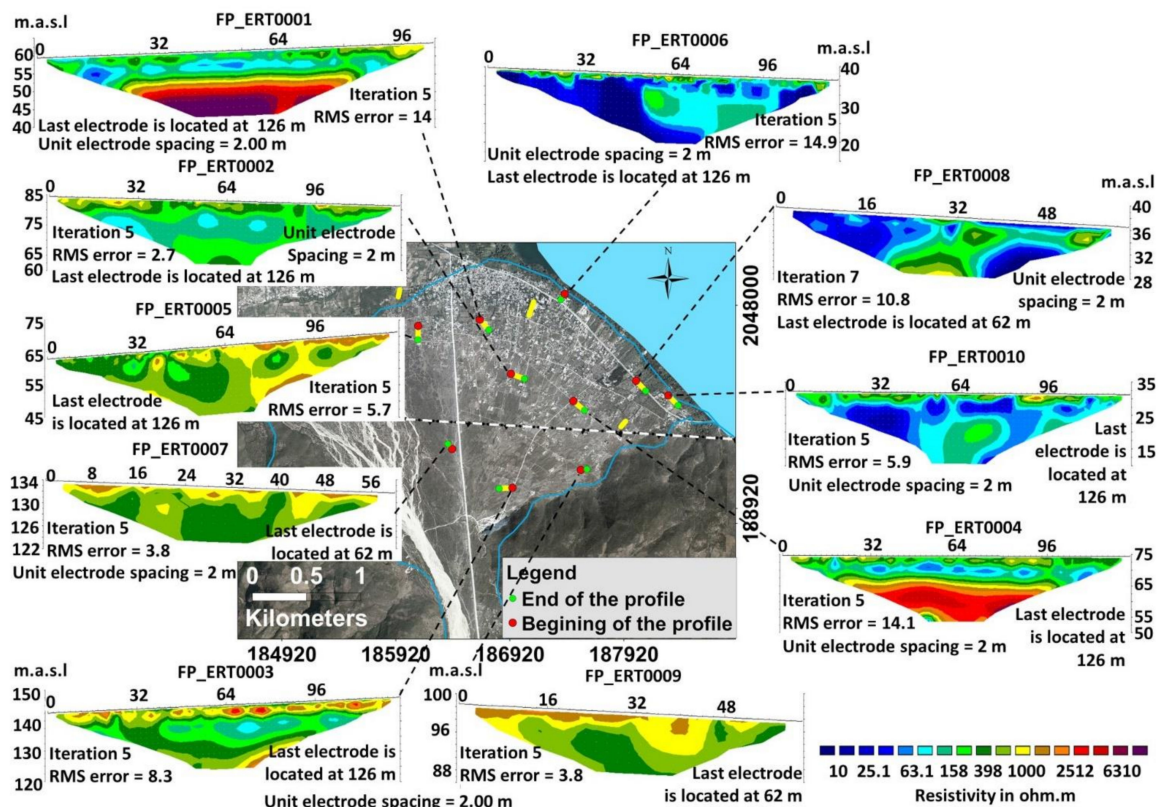

Figure 4. Examples of ERT profiles completed on the alluvial fan in the eastern part of Fond Parisien.

The moderate resistivity areas (70–1000 Ωm) are essentially located within the village (see lower left sections in Figure 4). The resistivity values along the sections are such that no relevant vertical contrast could be detected, with the exception of the two ERT FP_ERT0001 and FP_ERT0004 on the alluvial fan. Most of the cross-sections generally show a variable distribution of medium resistivity values characterising medium-dry soils with embedded stones of higher resistivity (>500 Ωm). The two aforementioned ERT sections marked by a stronger vertical resistivity variation, FP_ERT0001 and FP_ ERT0004, both display a shallow 10 m thick low-resistivity layer (40–600 Ωm) on top of a high-resistivity layer (>>1000 Ωm). Given that the neighbouring ERT profiles show more or less the same investigation depth (20–25 m) and did not reach the bedrock, this latter could have an irregular structure, being generally deeper than 20 m, besides a few zones like those investigated by the FP_ERT0001 and FP_ERT0004 profiles.

4.2. Seismic Surveys

1D Shear wave velocity (Vs) profiles were determined through MASW processing of the collected seismic data. The resulting Vs profiles show shear wave velocities of 200 to 850 m/s over the first 15 m.

An overview map of Vs profiles of the village "La Source" is shown in Figure 5. These Vs logs show that the upper and central parts of the alluvial fan are marked by shear velocity values of 580 to 860 m/s within the upper 15 m of soils (that could be investigated with the given seismic profiles). These values show that the alluvial fan is made of relatively dense rocky material. Closer to Lake Azuei, the Vs logs display values

between 280–640 m/s, with the lowest values of around 300 m/s obtained for the lakeshore typical marked by the presence of finer material. For all prospected sites an average Vs15 shear wave velocity over the first 15 m was calculated and represented by a specific color in the map shown in the central part of Figure 5.
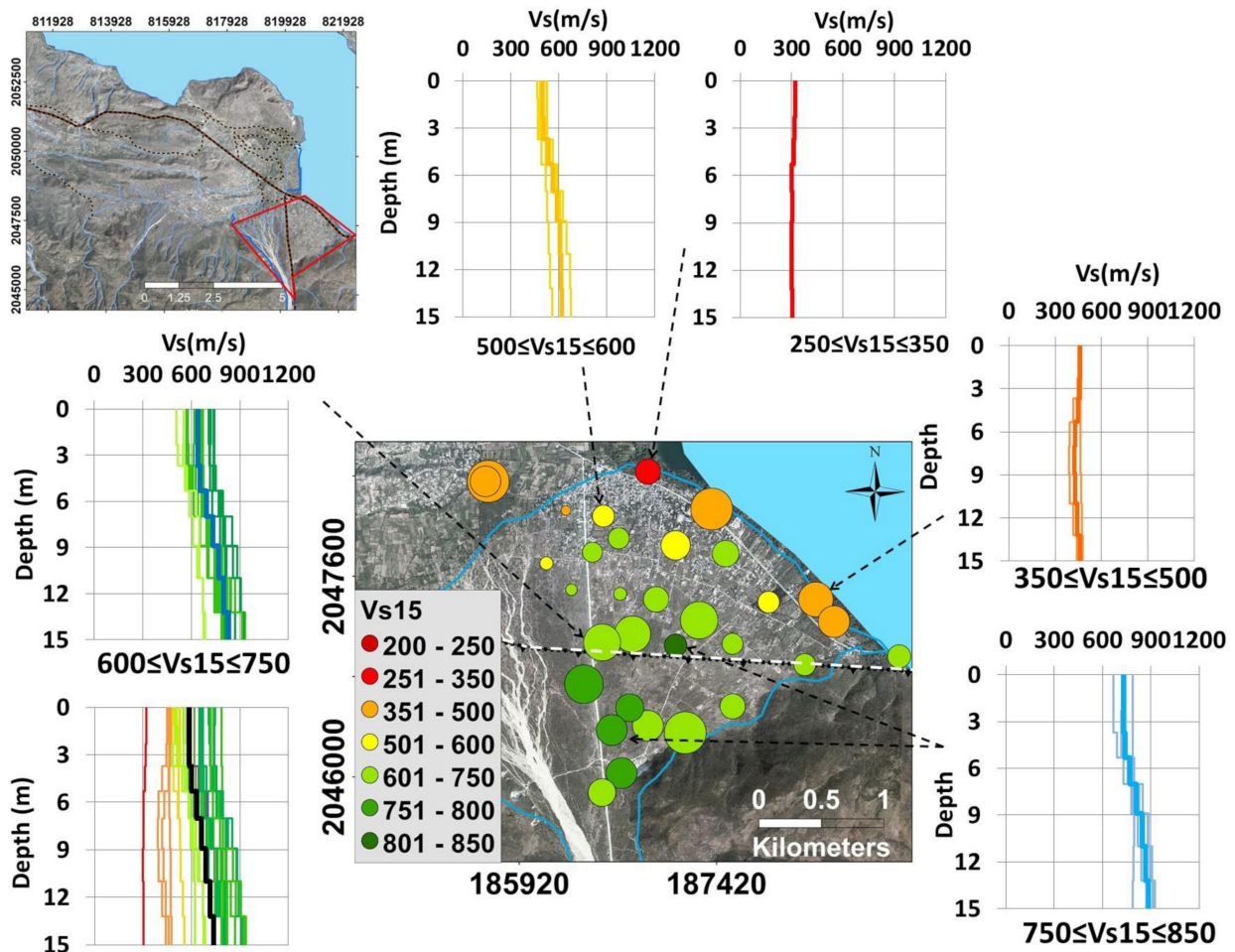

Figure 5. Vs profiles determined for the village "La Source" and the alluvial fan (down to a depth of 15 m). All profiles in this area are summarized in the lower left corner with an average Vs log of this area outlined in black. Average Vs15 values are represented in the central map by colors for each investigated site. See also the approximate location of the EPG Fault.

In Figure 6, Vs15 results (respecting the limit of the investigation depth of 15–20 m) are shown for the central and western parts of Fond Parisien. This larger map presents Vs15 values roughly in the same range as the smaller area around the village "La Source". Still, somewhat smaller Vs values (even below 200 m/s near the surface) could be measured in the sedimentary basin and near its western border (see location of red and dark red logs and corresponding Vs15 values in the central-eastern part of the map in Figure 6. The highest Vs15 values (>700 m/s) measured in these parts are, however, slightly smaller than those obtained in the upper part of the alluvial fan near the mountain range (Vs15 > 800 m/s). A first rough distribution pattern of Vs15 values can be outlined on the basis of the map in Figure 6: medium-high Vs15 values (400–750 m/s) mark the northwestern (closer to the lake) and southwestern parts (closer to the mountains) of the area, while lower values were measured in the central E-W elongated zone of Fond Parisien (250 < Vs15 < 500 m/s, with some local exceptions where sites present slightly higher values). Both, the maps in Figures 5 and 6 show gradient Vs15 values across the approximate EPG Fault zone, from higher values in the South to lower values in the North.
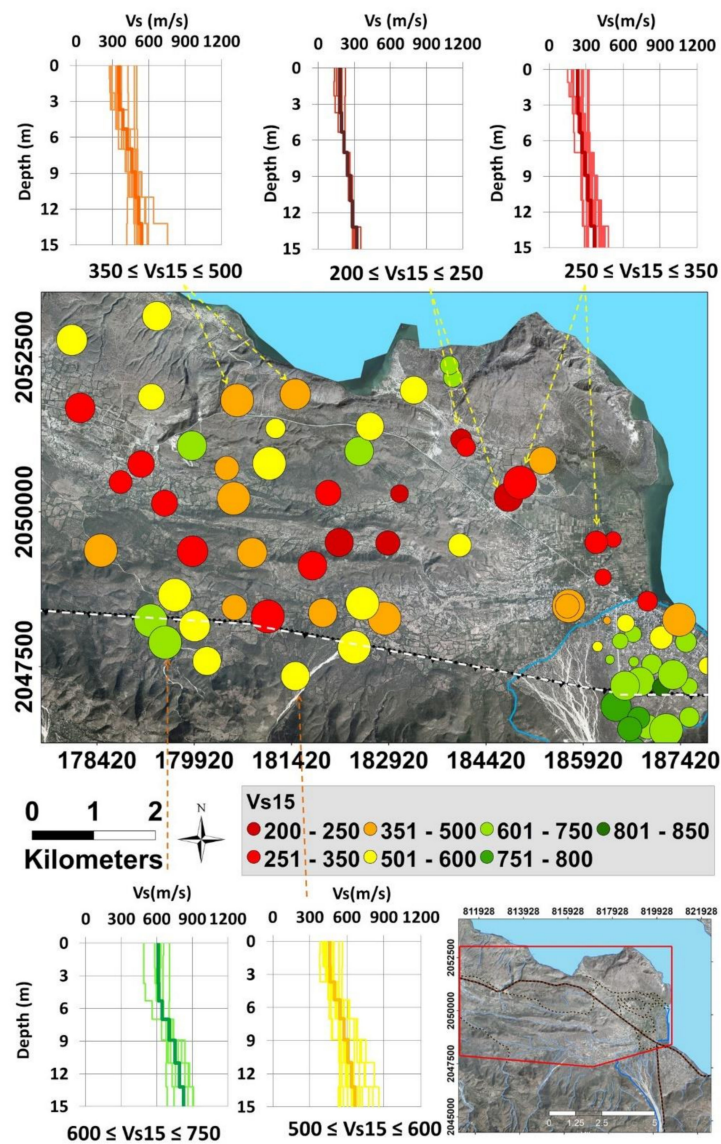
Figure 6. Vs profiles determined for the central and western part of Fond Parisien (down to a depth of 15 m). Vs15 values are represented in the central map by colors for each investigated site. See also the approximate location of the EPG Fault.

4.3. HVSR Results

The analysis of the ambient noise data in terms of HVSR was performed with the Geopsy software [43], within the frequency range between 0.25 and 25 Hz, taking into account the criteria of clarity and reliability of the measured peaks recommended by the "Site Effects Assessment using Ambient Excitations" (SESAME) project [36]. For each component, the fast Fourier transform was computed and a Konno–Ohmachi [44] smoothing scheme with a power b = 40 was applied to the Fourier spectra. Then, the ratio between the Fourier spectrum of the mean of the horizontal component and that of the vertical component was executed. Figure 7 below presents the HVSR results for the area of the alluvial fan, both in terms of computed HVSR curves and of interpreted fundamental resonance frequency and corresponding peak amplitude shown in the central map, respectively, through the color and the size of the circle.
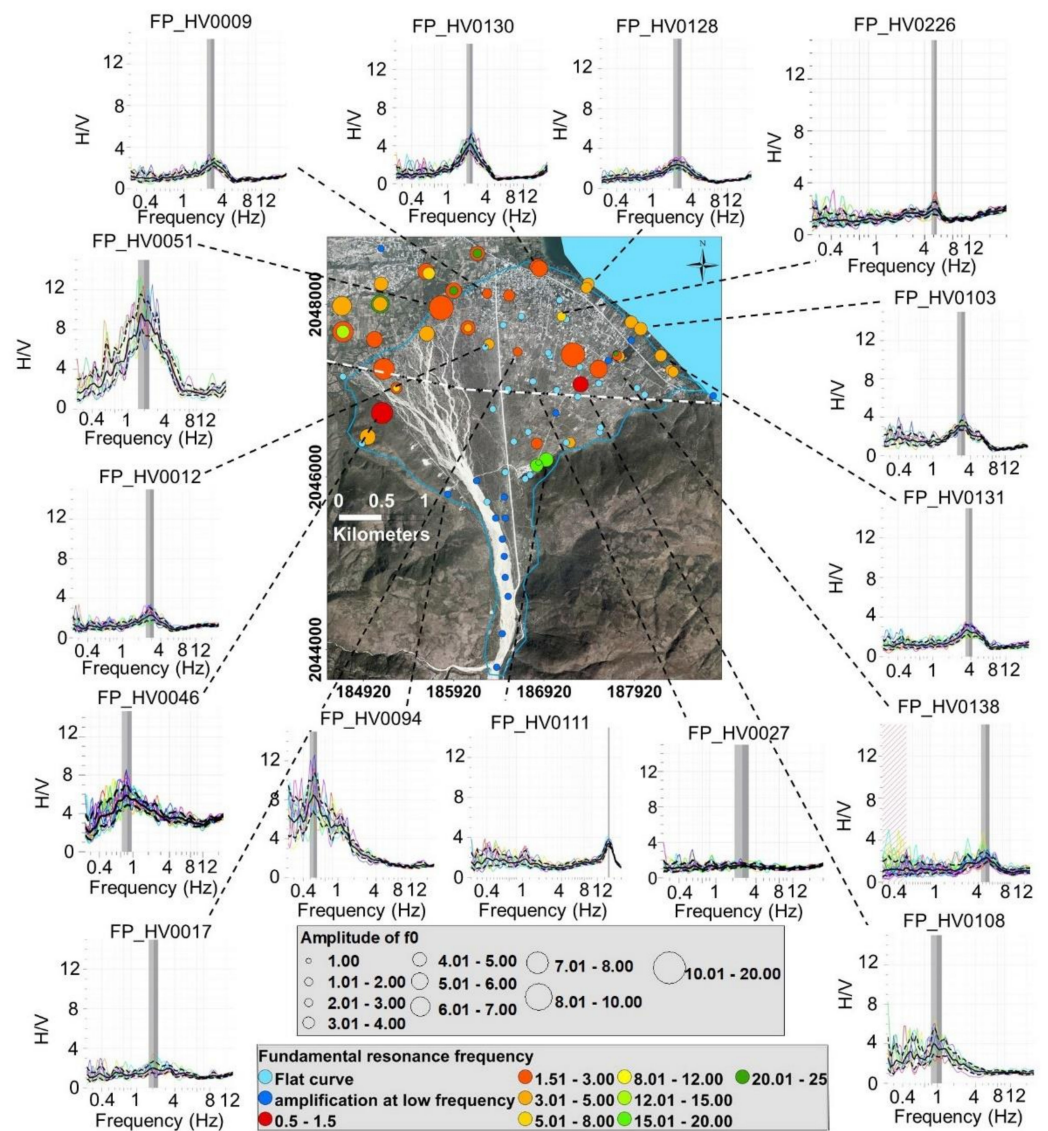
Figure 7. Examples of HVSR results obtained for ambient noise measurements completed on/near the alluvial fan. Circles on the central map indicate the resonance frequency, f0 (color), and amplitude of the f0 peak (size of circle).

It can be seen that the area of Fond Parisien is characterized by a large variability both in terms of HVSR resonance frequency and amplitude. The resonance frequencies range from 0.7 to 22.5 Hz and amplitude values are between 1.7 and 10. Focusing on the alluvial fan area and the village "La Source" located on its lower part, we first notice that the HVSR results obtained for the western and northern borders of the fan are marked by medium-size peaks at resonance frequencies of 3–6 Hz. In the central part of the alluvial fan, either clear peaks (amplitude >>2) at a lower frequency (< 4Hz) were obtained or no clear peak at all (see numerous light blue points plotted in this area in the map in Figure 7). Those flat H/V curves reflect low to inexistent impedance or velocity contrast between the shallow and the deeper layers. Additionally, HVSR curves presenting low-frequency peaks with amplitudes marked by a high standard deviation were computed for several sites, especially for those located along the river in the southern part; those are either due to the effect of wind or to the poor contact between the sensor and the unconsolidated stones and gravels that compose the river bed [31,45]. The lower resonance frequencies outlined for the central part of the alluvial fan compared to the sites near its border most likely indicate the larger thickness of the alluvia in the middle part of the fan. The observation

of numerous flat HVSR curves in the same zone marks the absence of any impedance contrast in the underground. This is in good agreement with some ERT results obtained in nearby places, which, within their investigation depth, also did not display any contact with underlying bedrock (while some fewer ERT sections clearly show a resistivity contrast at depth, at the contact with the bedrock).

Figure 8 presents an overview of all HVSR results mapped over the target region, presented in terms of fundamental resonance frequency (color of circle) and the corresponding peak amplitude (size of circle) and azimuth (double arrow—oriented according to the direction of maximum shaking amplitude—see azimuth-frequency HVSR graphs around the map). Just as the frequency and amplitude values, the related azimuth information computed from the ambient noise data also reveals large variations of the main wave field orientation. The most constant, roughly E-W oriented HVSR azimuth for medium-sized peaks at an average resonance frequency of 2–4 Hz, can be observed along the EPG Fault zone. This E-W azimuth trend is observed for different resonance frequencies and amplitudes, which allows us to rule out the possibility of a unique source contributing to this azimuth. It possibly can be explained by the presence of E-W elongated topographic features and parallel geological structure in this area. Such an influence of the free surface or the subsurface on the shaking azimuth (particularly in the case of basins) has been proven by several studies (e.g., Burjanek et al. [46]). Given the proximity of these measurement points to the fault trace, this preferential azimuth is best explained by the polarization of the wavefield next to this structure marked by a high structural anisotropy. In the North of the fault zone, in the central folded area, the wave field scattering phenomenon prevails over the polarization so that no azimuth predominance could be outlined. The wavefield scattering is caused by the multiple orientations of the layers in this folded area.
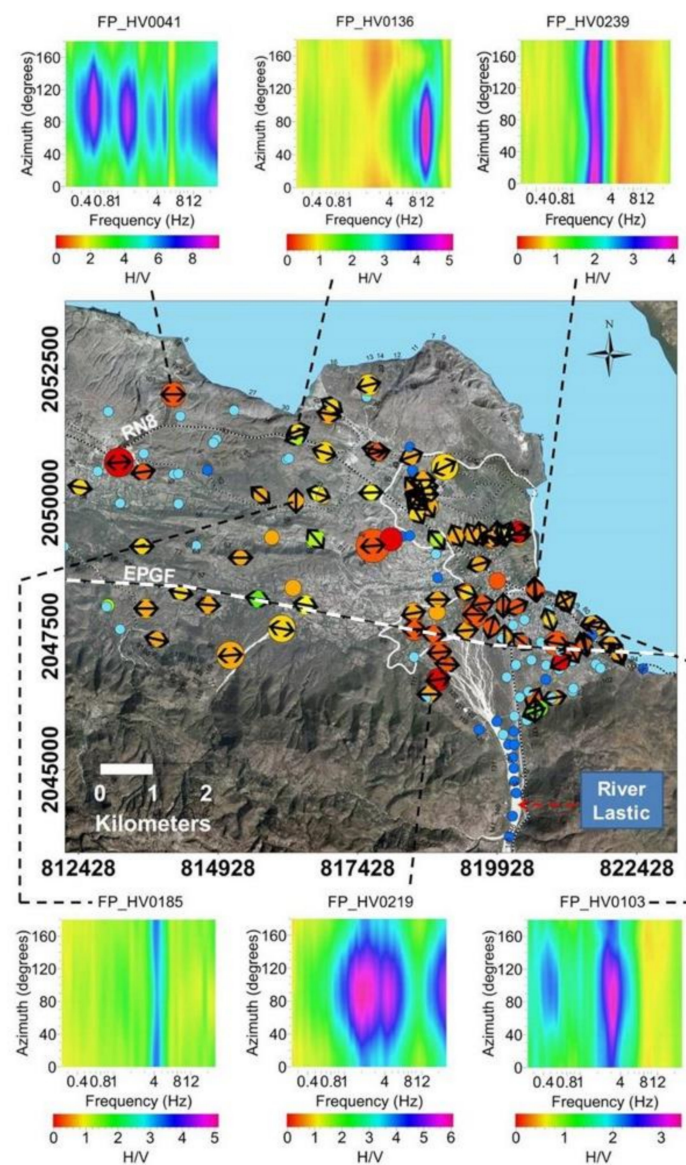
Figure 8. Azimuth analysis of the HVSR measurements performed in Fond Parisien. Graphs on top and at the bottom show the amplitude distribution over frequency and azimuth for six measurements. The double arrow on top of the f0-amplitude circles (see legend in the previous Figure 7) represents the preferential shaking orientation (of ambient noise).

4.4. Standard Spectral Ratio Results

4.4.1. Earthquake Data

We initially considered the identified earthquakes which are recorded by all the stations of the temporary network. Then, we selected the events recorded at the NM reference station as well as by another station of the network at least. The application of the SSR method supposes that the effects of source and propagation are identical between stations. This implies that the distance between the studied and the reference station is small compared to the distance between the epicentre and the reference station. In the case of Fond Parisien, the maximum distance between the different stations of the array was about 5 km (see the blue stars in Figure 3), and we selected 35 km as the threshold value for the minimum array—epicentre distance. Then, we proceeded to a rough assessment of the epicentre distance for each event. The epicentre distance was computed by applying a factor of 7.5 to the P-S waves delay time, ts-tp, already used by Havenith et al. [47]. It is however important to note that this is a very rough estimation, as we only require

an approximation of the epicenters for our purpose. Finally, 14 detected events with an estimated epicentre distance higher than the threshold value were pre-selected for later processing. The selected events are listed in Table 1, whereas examples of the seismograms for one event recorded at each station are shown in Figure 9. From this list, we used the signals of seven earthquakes detected at the four installed seismic stations for the SSR analysis.

Table 1. List of the 14 earthquakes recorded by the four stations in Fond Parisien; seven events recorded (R) by all stations were used for the SSR computations (not recorded is marked by "NO"). The geographical coordinates (latitude and longitude) are in decimal degree WGS 1984. Tp-Ts is the epicentre distance which corresponds to the delay time between the P and S waves.

| Date	Time	CH	LH	MN	NM	Tp-Ts (s)	Epicentral Distance (m)
05/28/2014	21:16:00	R	R	NO	R	26.45	198.375
06/02/2014	01:01:46	R	R	NO	R	20.69	155.175
21/06/2014	06:07:14	R	R	R	R	6.94	52.05
21/06/2014	14:32:46	NO	NO	R	R	4.63	34.725
21/06/2014	17:34:35	R	R	R	R	26	195
21/06/2014	23:06:54	R	R	R	R	3.295	24.7125
22/06/2014	05:58:05	Very noisy	R	R	R	5.1	38.25
25/06/2014	08:09:42	R	NO	R	R	22.47	168.525
27/06/2014	07:55:25	R	NO	R	R	3.95	29.625
29/06/2014	06:11:47	R	R	R	R	5.74	43.05
29/06/2014	18:10:45	R	R	R	R	1.35	10.125
07/02/2014	12:09:47	R	R	R	R	3.66	27.45
03/08/2014	04:41:00	R	R	R	R	2.27	17.025
09/08/2014	15:28:03	R	Uninstalled	R	R	21.99	164.925
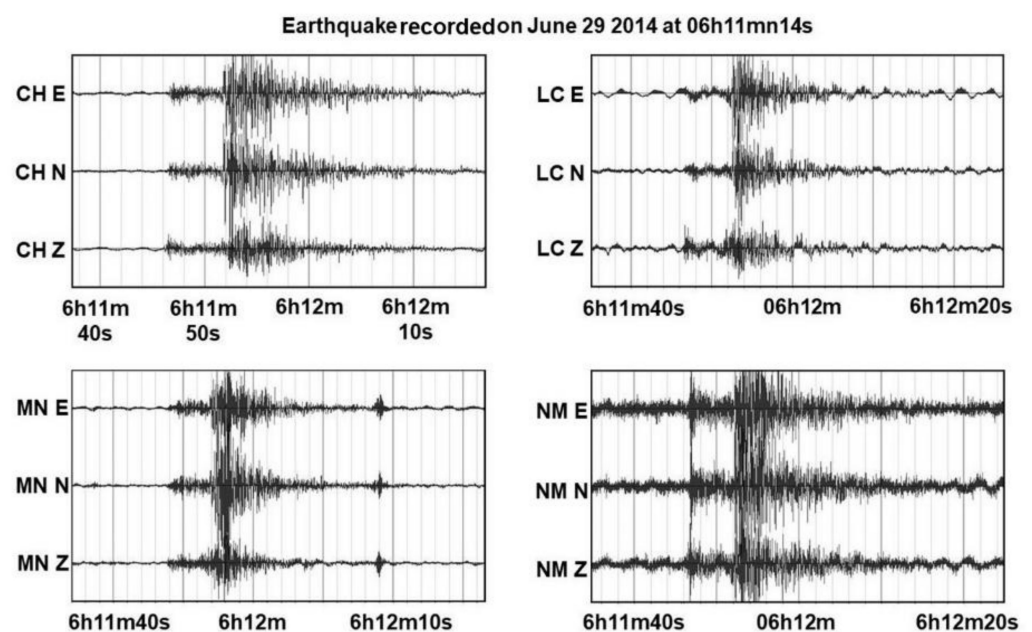
Figure 9. Seismograms (EW, NS and Z components) of the same earthquake recorded by the four temporary stations installed in Fond Parisien.

4.4.2. The Reference Station

Above, we indicated that the most appropriate reference station would most likely be the one in the South of the village "La Source", closer to the "Massif de la Selle", called NM (see location in Figure 3). Below, in Figure 10, we present HVSR measurement results for the NM site, using Tromino and seismic station recordings (both ambient noise and earthquake measurements, applied to S-wave windows).
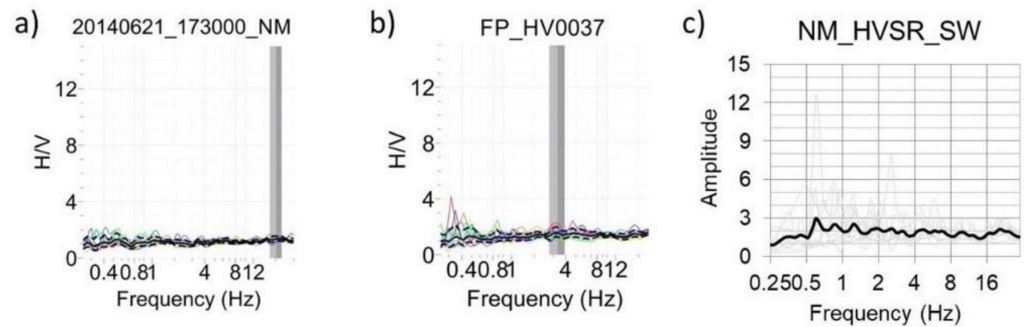

Figure 10. (**a**) HVSR curves from the Tromino single station measurements completed near the NM site; (**b**) HVSR results for the ambient noise recorded by the NM station; (**c**) HVSR curves computed from S-wave windows of earthquake recordings.

The amplitudes of both ambient noise and earthquake shaking HVSR curves are quite low and the curves do not display any particular peak, at least not within the frequency range of 1–10 Hz (a small peak appears at 0.6 Hz on the NM_HVSR_SW graph, but which is too low frequency to be indicative of any surface layer amplification).

4.4.3. Amplification Estimates

SSRs were computed on the basis of the whole S-wave window (averaged for both horizontal components, EW and NS, when not specified) recorded at each station. First, for each component of extracted S-wave, we computed the fast Fourier transform and we applied a Konno–Ohmachi smoothing scheme with a power b = 40 to the Fourier spectra. Then, the ratio between the Fourier spectrum of the target site and that of the reference site was executed component by component. The average of the SSR for the seven earthquakes which were recorded at the four stations was finally determined for each station.

Below we show HVSR and SSR results for CH station (for the other two non-reference stations, results are shown in the annex, in Figures A1 and A2). The station CH was installed in the eastern part of the alluvial fan, near the border of the lake where soft soil facies similar to those in the basin can be found. This zone is marked by an HVSR peak (computed both from nearby Tromino ambient noise and from seismic station recordings, in Figure 11a,b) at 4–5 Hz with an amplitude varying between 2.5 and 4. This peak frequency, denoted by the noise HVSR curves, is very clear in the S-wave HVSR curves shown in Figure 11c, where even a wide plateau-like peak between 0.6 and 6 Hz can be observed. Those plateau results from a combination of a small broad peak at 0.6–2 Hz and one at 2.5–7.5 Hz. The amplitude of these bumps, of about 3, is approximately the same as for the ambient noise HVSR. The SSR curves in Figure 11d rather confirm the results of the ambient noise HVSR, clearly highlighting the peak at 4 Hz; the broad peak between 0.6–2.5 Hz in the S-wave HVSR here becomes a minor peak between 1–2 Hz, and the SSR also show some smaller broad peak between 6–14 Hz. Considering all results, the peak at 4 Hz with an amplitude of 3 can be considered as the main resonance peak—noting that in this case the simple ambient noise HVSR predicted quite well both the frequency (as expected) and the amplitude (of about 3) of the shaking resonance of the CH site.
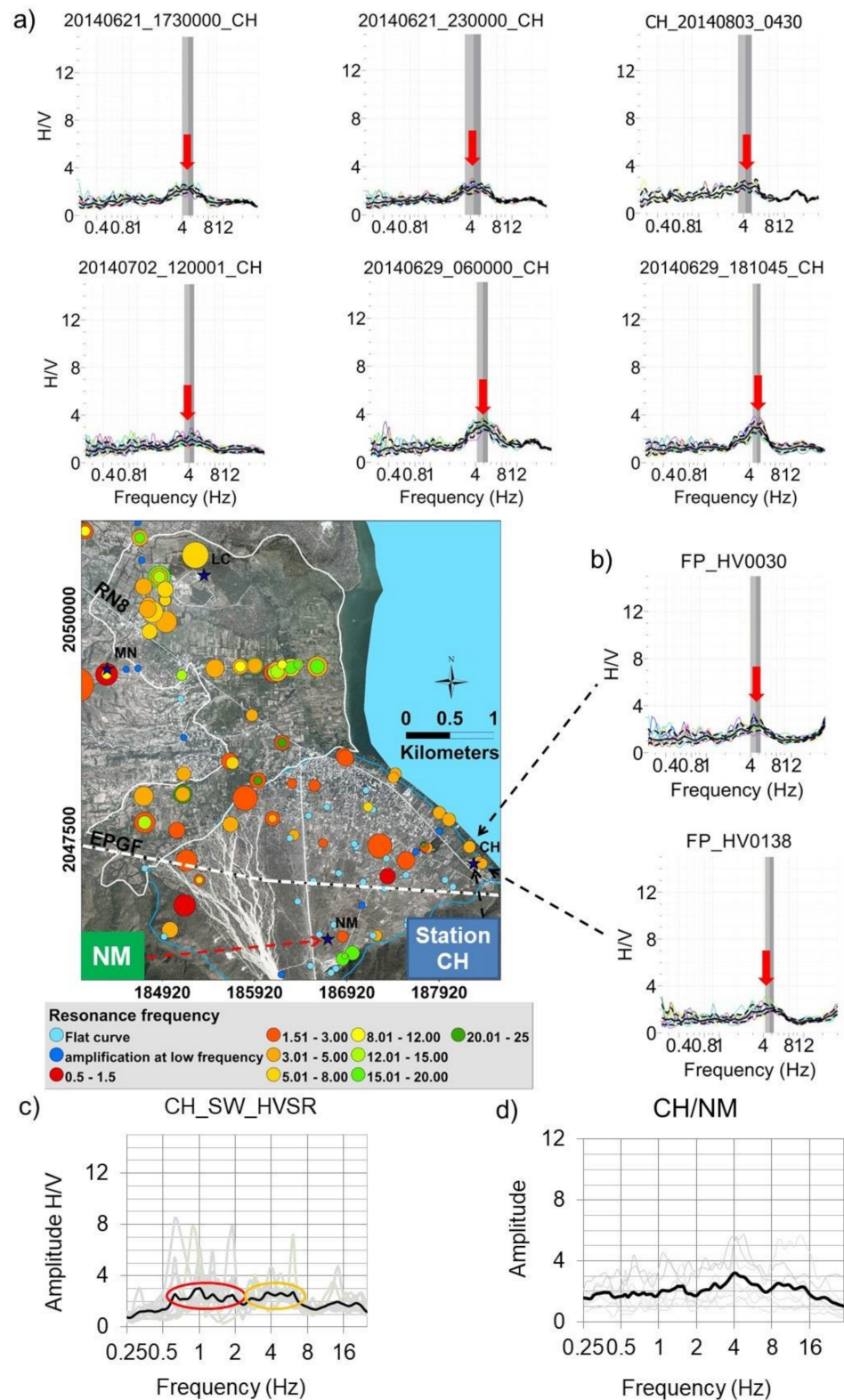
Figure 11. Spectral ratio curves computed for the site located close to the eastern border of the alluvial fan, near Lake Azuei (the map, with white solid line delimiting the sedimentary basin, shows the HVSR results for that zone in terms of resonance frequencies and amplitude as colored circles of different sizes; see also Figure 7 for scales): (**a**) ambient noise HVSR curves for station CH records; (**b**) Tromino ambient noise HVSR curves; (**c**) and (**d**) respectively the earthquake HVSR and SSR curves (the latter using S-wave window spectra of NM station as reference). Red arrows indicate the fundamental resonance frequency. Red and orange ellipses show broad frequency peaks. Additional information cab be found in (Figures A1 and A2).

For the MN station, which is located on a slope and in the area of the Ganthier fold, a sharp peak can be observed at 8 Hz (see annex, Figure A1) considering all the obtained spectral ratio curves (see annex, Figure A1a–d). However, as can be seen in the figure in the annex, the amplitude of these peaks is clearly lower for the noise spectral ratios (~3–4) than for the HVSR and SSR computed for the S-wave windows of earthquake recordings (amplitude of 6). Differently from the HVSR computed with the data of the MN station, those of the Tromino exhibit some high disturbance at low frequency. Such perturbations may be related to the effect of the wind that was often felt in that area (station MN was protected from weather effects).

The station LC located in the northern part of the sedimentary basin is marked by a large variation between the curves from noise and the earthquake data (Figure A2 in the annex). Its HVSR curves are quite flat with an amplitude slightly below 1 for frequencies between 1 Hz and 7 Hz. A similar trend is observed for the SSR curve for frequencies higher than 2 Hz. However, this latter exhibits an amplification at low frequency including small peaks at 0.7 and 0.9 Hz.

The results obtained from the data recorded by the temporary seismic network thus differ from one station to another. CH and MN are the stations for which a clear resonance peak can be observed (shown by most spectral ratios, using both ambient noise and S-wave earthquake data). However, for station LC, ambient noise HVSR completely differs from those of the nearest Tromino measurements (compare Figure A2a with Figure A2b in the annex) which systematically show a clear resonance peak in the range of 4 to 8 Hz—barely seen in LC ambient noise HVSR but appears on the S-wave HVSR at 6–7 Hz. Some of the Tromino HVSR curves are even marked by a double or triple peak. It is however worth noting that these Tromino measurements were not recorded exactly in the same place as the station LC. Interestingly, the SSR curve (see Figure A2d in the annex) does not display any clear resonance peak above 1 Hz. As indicated above, its shape is more or less similar to the LC ambient noise HVSR curves except that it presents some small peaks at a lower frequency.

With the exception of the station LC, a quite good agreement in terms of the resonance frequency is observed between the average SSR and the HVSR curves. Some similarities can also be observed for the directional SSR. Indeed, apart from the station CH which seems to show a slight 1–2 Hz amplification for the E-W SSR that is not present on the N-S SSR, the E-W and N-S SSR curves show, for all the other stations, resonance peaks at roughly the same frequency and with amplitudes similar to those of the corresponding average curves (comparing the EW and NS SSR curves in Figure 12 with the average SSR curves in Figures 11d, A1d and A2d). This similarity reflects the absence of preferential orientation of the seismic wavefield for these sites (MN and LC) as already indicated by the directional HVSR results obtained from the ambient noise Tromino data (Figure 8), which did not show any preferential azimuth in the North of the fault trace. However, as CH station is located very close to the EPGF trace, the differences in the NS and EW SSR curves, with an additional peak on the EW SSR, could be explained by the location near the fault as we already observed preferential EW shaking from HVSR measurements in the proximity of the EPGF zone shown in Figure 8.
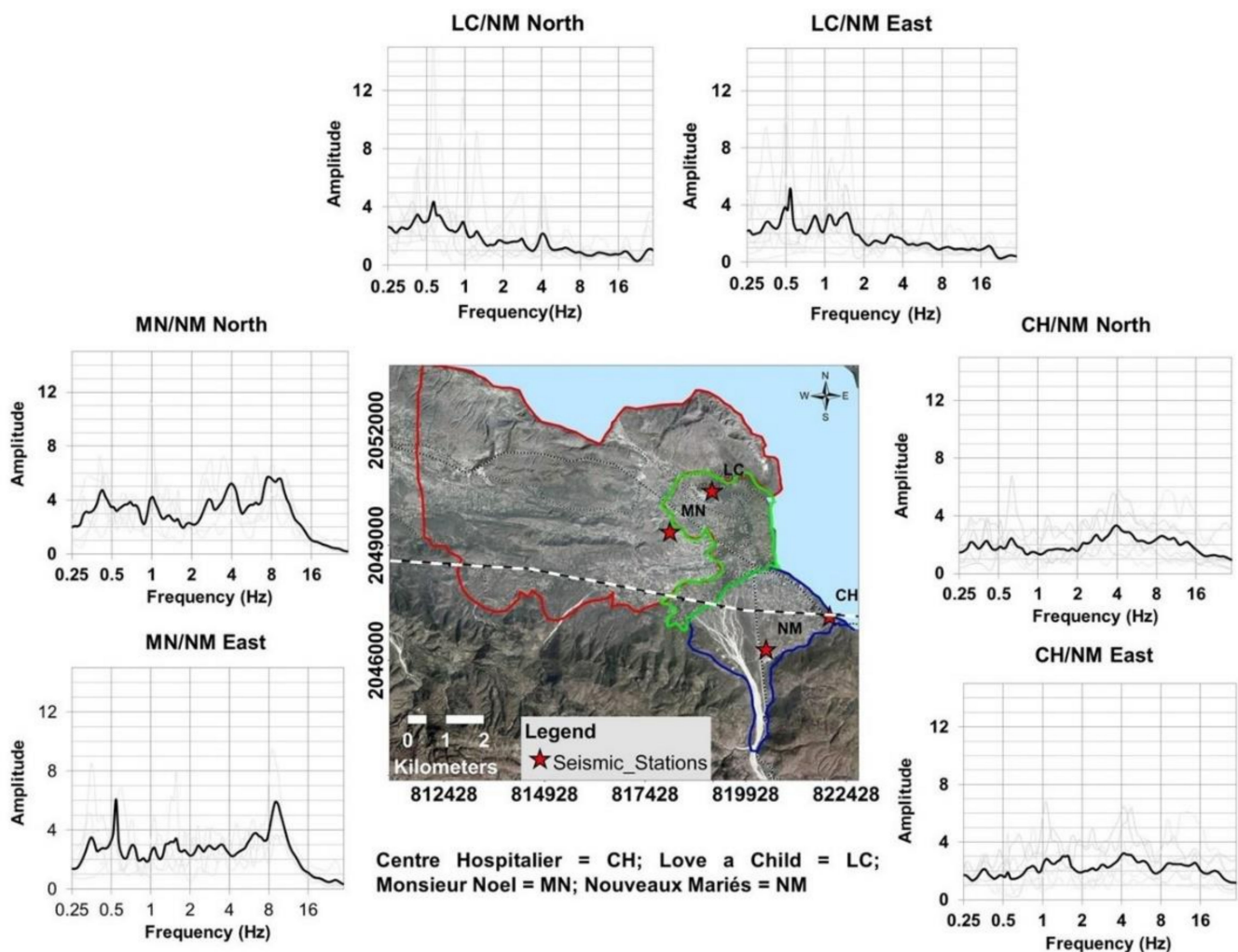
Figure 12. Distinct EW (East) and NS (North) SSR for the stations CH, MN and LC, using NM as reference. The black line marks the EPGF trace.

It is also interesting to observe the much lower amplitude displayed by the SSR EW and NS curves at station CH compared to the one at the MN station. The amplitudes at the MN station exceed those at the CH site by a factor of almost two. The very high amplification factor showed by the MN SSR curve is not only related to topographical effects but may also have a tectonic origin. Given that this station was installed within the area of the Ganthier fold, a 2D or 3D effect (due to the fold) might contribute to this stronger amplification, as discussed further below.

5. From Integration to Mapping and Discussion

5.1. Integration of Results

The previous analyses showed that for most of the investigated areas a good agreement exists between the results obtained from the different applied geophysical methods. For instance, the areas marked by the highest seismic velocities (e.g., in the Southeast on the alluvial fan) are those where the largest resistivities were observed. Likewise, in many places, the low seismic velocity zones correspond to areas of low resistivity. In addition, some of the higher seismic velocity zones are also characterized by flat HVSR curves, thus suggesting that there is no or only a slight impedance contrast between the shallow and the deeper layers. This is the case of the alluvial fan hosting the village "La Source". There, the high seismic velocity zones are also marked by flat HVSR curves and indicate that these alluvial materials coming from the massif should be sufficiently consolidated so that their impedance does not differ from that of the underlying bedrock. However, most of the

velocity models also either present constant or gradually increasing velocities with depth. Considering the pattern of the corresponding ERT models which globally do not exhibit any vertical variation, we interpret the gradually increasing velocities as being related to an increase of the material compactness (see lower ERT sections in Figure 13). More precisely, the Vs logs presented in that figure show that the upper and central parts of the alluvial fan are marked by shear velocity values of 600 to 850 m/s within the upper 15 m of soils (that could be investigated with the given seismic profiles). The ERT sections further show that the corresponding relatively dense rocky material is medium dry (marked by medium resistivity values) and that locally the bedrock can be reached at a depth of less than 12 m—as indicated above (for the H/V results), some buried bedrock ridges might have been detected in those places (see upper ERT in Figure 13 and lower ERT profile in Figure 14). Moreover, the low amplitude peak at a low fundamental resonance frequency value of 2.5–3 Hz shown by the HVSR curves indicates the existence of a deeper contrast that could not be reached by the ERT profiles. Indeed, considering for example the results related to the ERT profile FP_ERT0004, the application of the formula h = Vs/(4*f0), with an average Vs of 500 m/s and the bedrock depth of 12 m shown by the ERT profile, provides an f0 value of about 11 Hz that is largely higher than the one of the corresponding FP_HV0008 measurement. Closer to Lake Azuei (upper part of Figure 14), the Vs log displays values between 280–320 m/s, typical for finer material. This finer material is supposedly partly water saturated as the nearby ERT profile presents very low resistivity values. Those sites closer to the lake also present clear resonance peaks on the HVSR curves, marking some impedance contrast at depth.
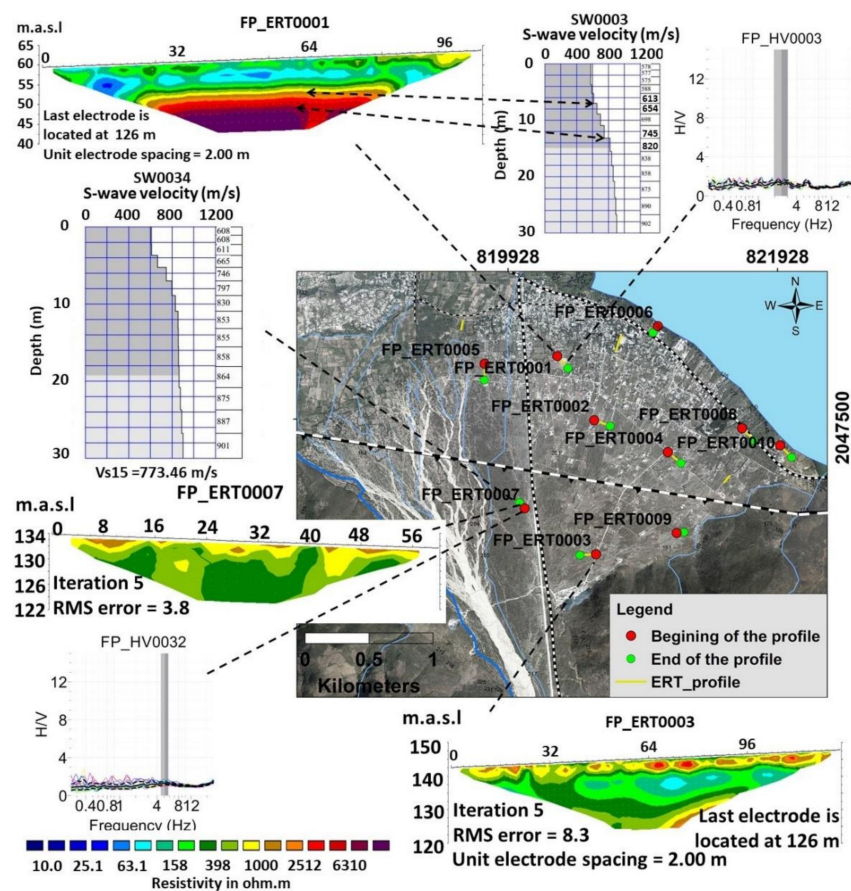

Figure 13. Comparison between ERT and MASW results for measurements completed on the central and upper parts of the alluvial fan.
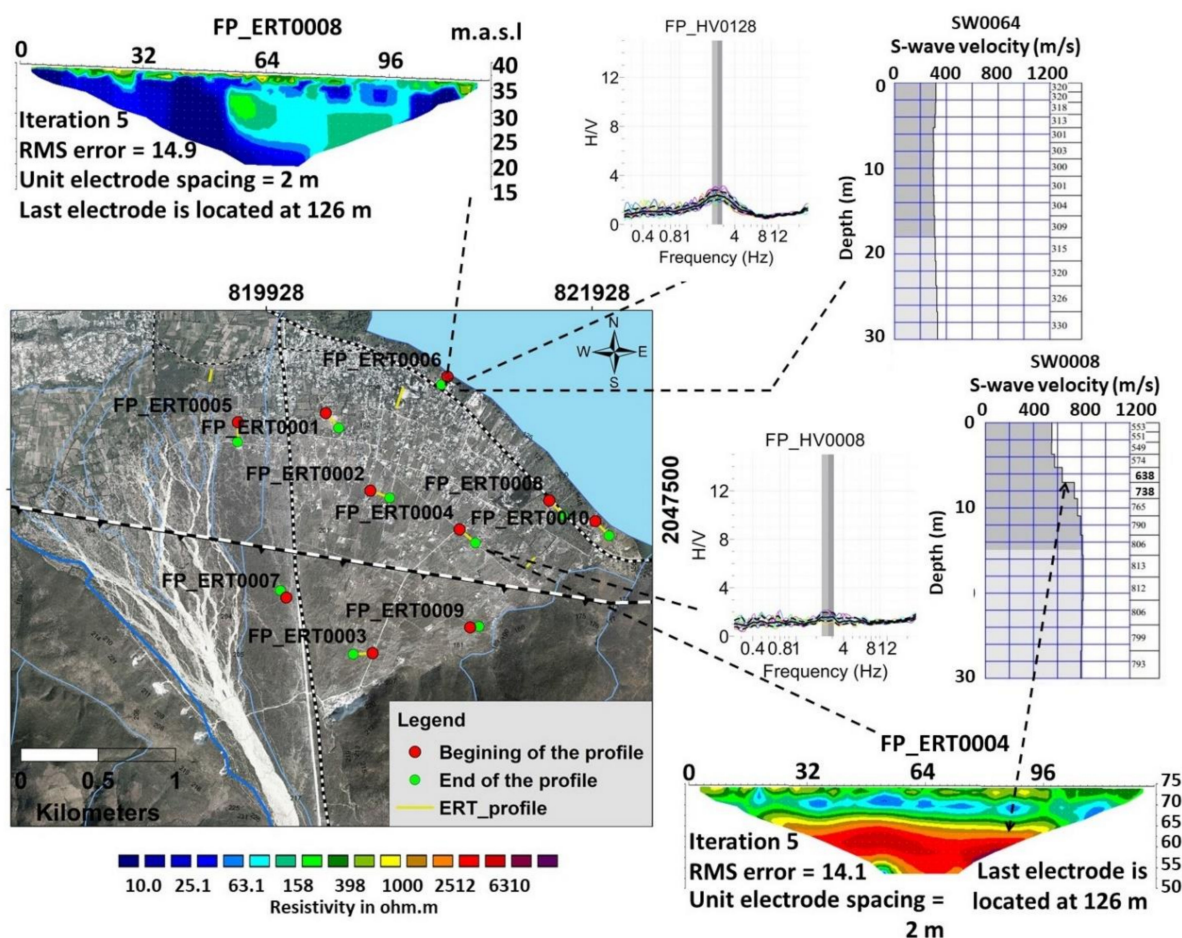
Figure 14. Comparison between ERT and MASW results for measurements completed on the lower part of the alluvial fan, near Lake Azuei.

The zones marked by both, very low resistivities and low S-wave velocities, are typically located within the sedimentary basin where the HVSR curves also highlight a sharp impedance contrast between shallow and deep layers. In these areas, the resistivities range from 0.5 m to 100 Ωm and the P-wave velocities vary between 195 m/s and 385 m/s, with values below 330 m/s in the eastern and central parts of the basin. As mentioned above, the sedimentary basin is composed of thin material deposits of clayey to silty type. In addition, the results of two standard penetrometer tests also carried out in the basin during of our investigating campaign (Figure 15b, left diagrams) indicate that the soils in the basin are poorly indurated with mean compactness ranging from 10 to 30 MPa, down to a depth of at least five meters. The very low resistivity and the low velocity in the basin may thus be attributed to the presence of these thin and soft sediments. Additionally, the subsurface should be characterized by a high saturation level over varying depths as the impedance contrast evidenced by the HVSR curves has not been detected by any of the ERT sections (even the profiles of 315 m length completed in the basin present resistivities of less than 60 Ωm down to a depth of more than 50 m). The combination of shallow layers made of fine material, poorly indurated and fully saturated hints at a locally increased liquefaction hazard in the so-called sedimentary basin.
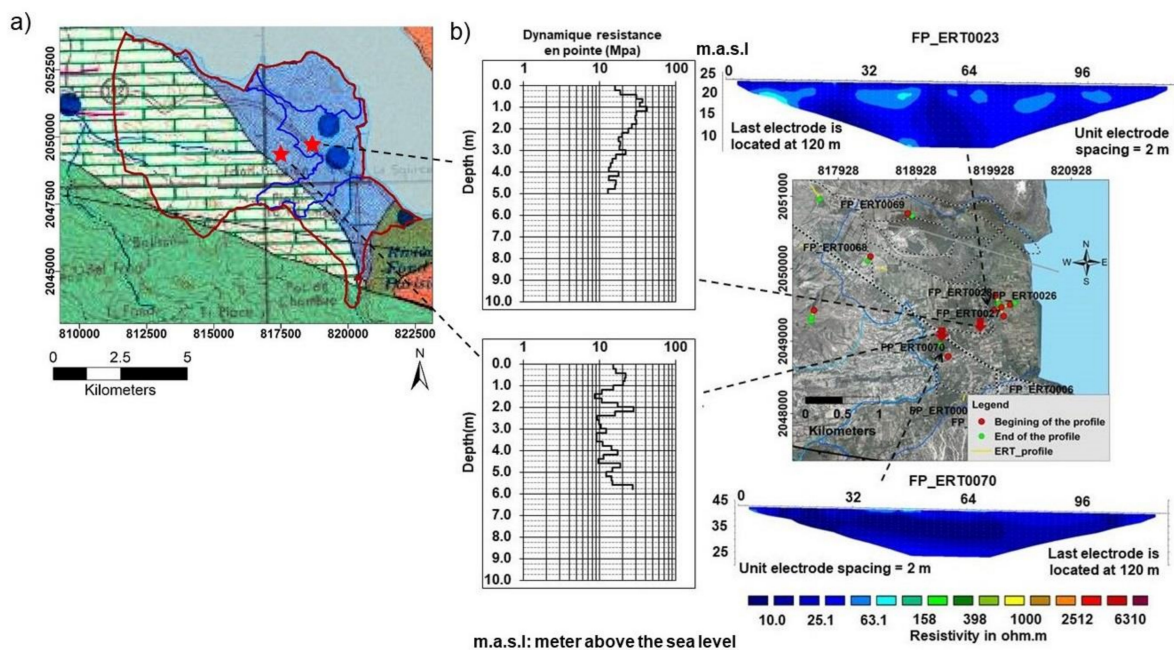
Figure 15. (**a**) Hydrogeological map (1/250,000) of Fond Parisien extracted from the hydrogeological map of Haiti—with blue zone indicating very shallow water table in soft sediments (see also stars locating the penetrograms and ERTs shown in (**b**). (**b**) Standard tests penetrometers realized in the sedimentary basin of Fond Parisien together with some ERT sections. The penetrograms reveal mean compactness ranging from 10 to 30 MPa over the 5 m thick investigated, thus denoting poorly compacted soils; a geotechnical borehole completed in the village "La Source" of Fond Parisien in the south of the lower ERT is shown in the annex in Figure A2.

From the analysis of the shape of the different velocity models, some changes from a shallow soft layer with velocity below 365 m/s to a deeper layer marked by larger velocities within a range not exceeding 750 m/s could be identified on some of the velocity models at varying depths. This contrast thereby corresponds to the change from thin sediments to a harder rock which is not yet the hard bedrock. For these profiles located near the northwestern boundary of the basin, the HVSR curves display a single fundamental resonance peak frequency in the range of 4.7 Hz to 6.4 Hz with an amplitude between 2.5 and 7.3. From the Vs logs obtained in the West and in the Southwest of the station LC, it can be seen that the interface depth varies between 21.4 m and 23.8 m. The assessment of this depth from the application of the relation $h = Vs/(4*f0)$ using an average velocity ranging from 220 to 485 m/s, provided values ranging from 12 m to 19 m.

5.2. Site Effect Distribution Maps

In order to better delineate the spatial distribution of site effects in the study area, HVSR and MASW results were interpolated. For the interpolation process, a stochastic method was used, i.e., the kriging tool implemented in the ArcGIS software. We chose the kriging method because it has the particularity to take into account the spatial dependence structure of the data. In addition, it is an exact interpolation method that restores the measured regionalized values to their respective observation sites. In order to apply the kriging method correctly, it is very important to specify the dependency structure of the random function. In our case, this latter is obtained from outputs of a geostatistical analysis previously performed using the R software. The results of this geostatistical analysis are represented by a semi-variogram which is a curve characterized by three parameters: the nugget effect, the major range and the partial sill. The nugget effect informs about the undetected variations while the major range and the partial sill are related to observable variations. These parameters are used as input parameters for kriging.

The interpolation maps produced by kriging provide the distribution of the values of the different parameters for the investigated area. Three maps were thus computed: the

shear wave velocity of the top 15 m (Vs15) map (Figure 16), the fundamental resonance frequency, f0, map (Figure 17a) and the corresponding peak amplitude map (Figure 17b).
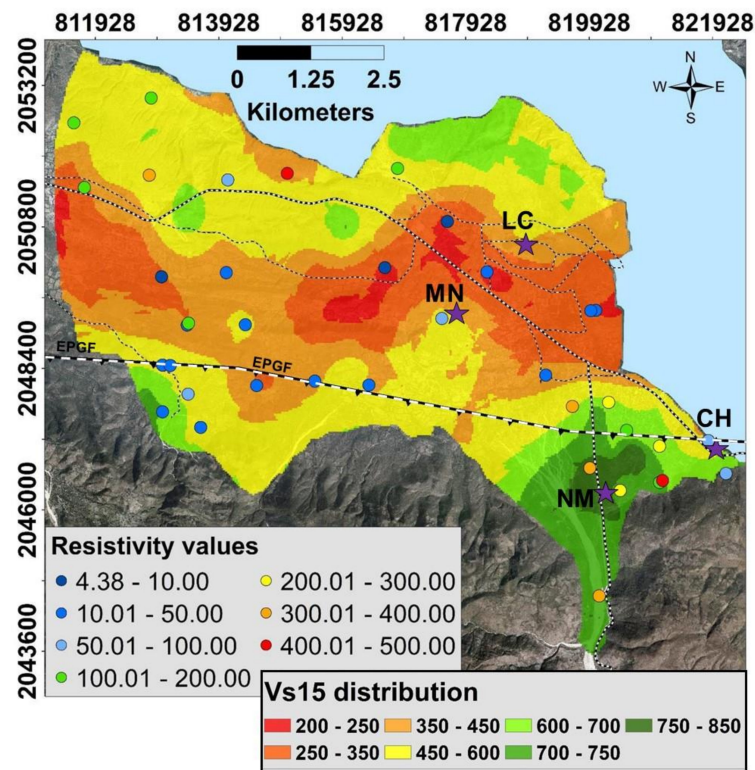

Figure 16. Map of shear wave velocity distribution in terms of Vs15 compared with local resistivity values averaged over the upper 15 m of the corresponding ERT profile.
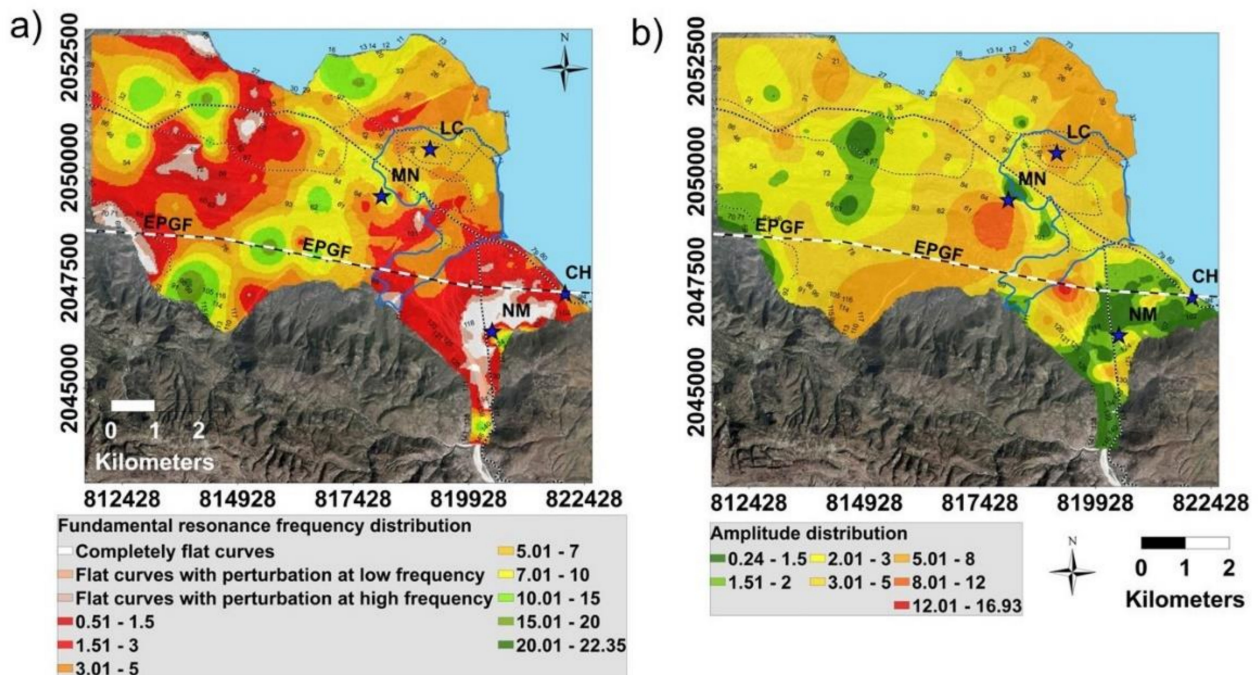

Figure 17. Maps of fundamental frequency, f0 (**a**) and corresponding peak amplitude (**b**) distribution. See also outline of EPGF (black, dashed) and of the sedimentary basin (green polygon).

The Vs15 map (Figure 16) highlights, in the central part of Fond Parisien, a low-velocity zone marked by Vs15 < 450 m/s that is elongated in the E-W direction. To the north and south of this zone, Vs15 values gradually increase to reach 650 m/s in the North (with the exception of a small low-velocity zone near the lake) and 850 m /s in the South. The general spatial trend of the shear wave velocity value variations is also similar to the spatial distribution pattern of the ERT results. This is shown by the resistivity values averaged over the upper 15 m of the ERT profiles plotted in terms of circles colored according to those resistivity values on top of the Vs15 distribution map. Indeed, the resistivity ranges are very low in the central E-W elongated zone which roughly corresponds to the central low Vs15 zone; however, in the northern and in the southern parts of Fond Parisien, resistivity values are moderate to high with the higher values found near and in the South of the village "La Source".

By comparing the Vs15 distribution (Figure 16) with the HVSR parameter (f0, amplitude) variation maps (Figure 17a,b), it can be seen that the higher velocity zone near and in the South of the village "La Source" roughly corresponds to the area marked by flat HVSR curves. The flatness of the HVSR in this part suggests no impedance contrast between the shallow and deeper layers (as it was also shown by the earthquake HVSR computed at the station NM installed in the area). However, in the North (close to the lake) and partly also in the West of this village, the zones are marked by shear wave velocity and resistivity values (Figure 16) lower than those in the rest of the village; these zones are probably covered by less consolidated (and also thinner) materials than those inside the village. Their clear and more or less sharp frequency peak at 2–5 Hz reveals the existence of an impedance contrast with regard to harder deeper soils, which is capable of generating significant amplification of the ground motion.

The relatively good agreement between the Vs15 and HVSR parameter distribution shown for the southeastern part is however not observed in all most other zones of the target region. Indeed, as presented by the map Figure 17a, the HVSR results reveal large variations of the fundamental resonance frequency without any spatial tendency (no E-W trending zone can be outlined). We interpret the clearer shape of the Vs15 distribution as being influenced by the regional tectonics related to the neighborhood of the roughly E-W trending EPGF. The higher variability of the frequency and corresponding peak amplitude values in that area show that the tectonics do less influence the local shaking resonance that is most likely more constrained by local surface layer thickness variations. In this regard, it can be noticed the sedimentary basin (blue polygon plotted on the maps in Figure 17) is better identified on the basis of the f0 (typically between 2–5 Hz) and peak amplitude (>2.5) distribution.

Combining the values of the Vs15, the fundamental resonance frequency (f0), the amplitude and the quality index of the frequency peak (that we qualitatively determined on the basis of the amplitude compared to the width of the peak), we mapped the site effect distribution across Fond Parisien (see Figure 18). A ground motion amplification level was associated with each of the sites where ambient noise data were recorded. The amplification level, referred to as the "Level of site effect", was defined according to the values of these four parameters in the considered point. For each parameter, the resulting values were grouped into several classes (see Table 2 in the annex below) on the basis of the ground motion amplification level which is usually associated with the values of the parameter. For example, in a given site, the ground motion amplification is generally considered as significant when the HVSR peak amplitude is higher than 2 and the resonance frequency is between 0.5 and 10 Hz, a stronger expected ground motion as the frequency is lower. Beyond 10 Hz, the peak frequencies are associated with moderate to slight site effects. Likewise, according to Johnson et al. [48], the shear wave velocity of the top 30 m (Vs_{30}) greater than 760 m/s and lower than 366 m/s, respectively, suggest a lower and a higher lithological site amplification potential. The values of the Vs_{15} (shear wave velocity over the top 15 m) parameter used in this study were classified following the recommendations of Johnson et al. [48]. Concerning the "quality index (QI)", the classification of its values

was done on the basis of the sharpness of the peak frequency (here, based on the ratio of peak amplitude by peak width).
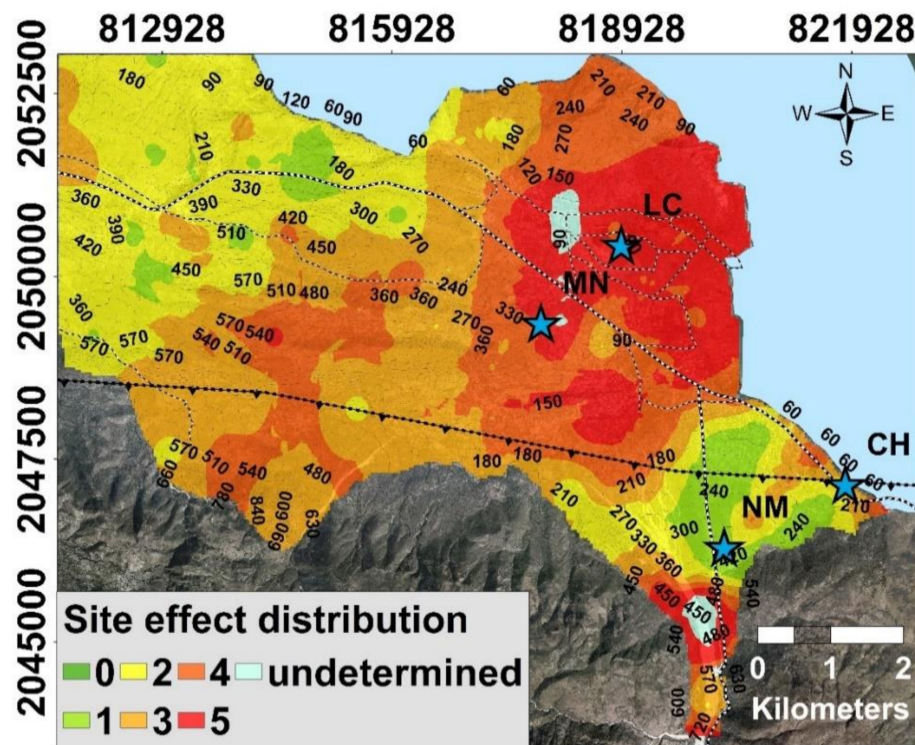

Figure 18. Map of the site effect distribution levels (0–1 represent no or very weak site effects, 4 to 5 marking strong site effects) in Fond Parisien. The classification is based on Equation. 1, and outlined in Tables 3 and 4.

Table 2. Classes of values defined for the different parameters with their respective reference number.

Vs15	Class of Vs$_{15}$	f0	Class of f0	A0	Class of A0	Index_f0	Class of Quality Index
<200	17	disturbance with high amplitude without frequency peak	−1	disturbance with high amplitude without frequency peak	−1	disturbance with high amplitude without frequency peak	−1
≤ 300	13	0.5 < f0 < 2	31			0.4 < QI < 5	11
		2 ≤ f0 < 5	29			0.1 < QI ≤ 0.4	7
300 < Vs15 < 400	11	5 ≤ f0 < 7	23	A0 > 3	2	0.05 ≤ QI ≤ 0.1	1
400 ≤ Vs15 < 450	7	7 < f0 ≤ 10				0	0
450 ≤ Vs15 < 600	5	10 < f0 ≤ 12					
600 ≤ Vs15 < 750	3	f0 ≥ 12	1	2 ≤ A0 ≤ 3	1		
Vs15 ≥ 750	1	No f0	0	A0 < 2	0		

Table 3. Classes of site effect obtained by the multiplication of the reference numbers parameter by parameter.

Class of Site Effect	Vs$_{15}$ (m/s)	f0 (Hz)	A0	Quality Index
site effect < 0		disturbance with high amplitude without frequency peak		
5000 < site effect < 11,000	≤ 375	0.5 < f0 < 6.5	A0 ≤ 3.5	0.3 < QI < 5
3000 < site effect < 5000	225 < Vs15 < 560		2.1 < A0 < 8.3	0.1 < QI ≤ 2.8
1500 < site effect < 3000	225 < Vs15 ≤ 670	1.9 ≤ f0 ≤ 11	2.05 ≤ A0 < 10	0.1 < QI < 1
600 < site effect < 1500	400 < Vs15 ≤ 700	1 < f0 < 8	2 ≤ A0 < 5.5	0.1 ≤ QI ≤ 0.61
13 < site effect ≤ 600	225 < Vs15 < 740	0.9 ≤ f0 ≤ 12	2.1 ≤ A0 < 5.9	0.05 ≤ QI ≤ 0.2
0 ≤ site effect ≤ 13	≤ 300	No f0 or f0 > 12	A0 < 2	≤ 1.4

Table 4. Levels of site effect.

Class of Site Effect	Level of Site Effect	Scale of Values
site effect < 0	Very strong site effect	5
5000 < site effect < 11,000	strong site effect	4
3000 < site effect < 5000	Significant site effect	3
1500 < site effect < 3000	Moderate site effect	2
600 < site effect < 1500	Slight site effect	1
13 < site effect ≤ 600	No site effect	0
0 ≤ site effect ≤ 13	Undetermined	6

Reference numbers were associated with the thus-defined classes. These reference numbers are distinct prime numbers thus ensuring that a calculated level of site amplification strictly corresponds to a unique class of site effects. Moreover, they are selected such that the higher numbers correspond to larger amplification potential (see Table 3). So, the higher the amplification potential, the larger will be the resulting product. The multiplication of the reference numbers, parameter by parameter, provides the level of site effects at each point, as expressed in the following equation, Equation (1):

$$Se = \zeta \times \alpha \times \vartheta \times \iota \tag{1}$$

where the variables ζ, α, ϑ and ι are respectively the class reference number of the frequency, the amplitude, the shear wave velocity and the quality index of the frequency peak for each Tromino HVSR measurement.

In order to represent more clearly the results, these products were afterwards identified by integers defining a scale of values where the higher integers (or class numbers) are attributed to the greater products. A detailed description of this scale is shown in Table 4.

It graduates from zero to five, the zero corresponding to the case where no site effects are expected while the integer or class five refers to the strongest level of amplification of the ground motion. A seventh class characterizes the undetermined situation mostly marked by a high amplitude at low frequency observed in some of the HVSR curves. These disturbances of high amplitude at low frequency cannot be associated with a reliable peak (as often related to wind effects or local anthropogenic noise), nevertheless, given their repeatability, they were represented in the result distribution anyway.

In concordance with the HVSR and Vs distribution maps, the resulted synthetic site effect distribution map shows the lower and higher potential of amplification of the ground motion respectively in the village "La Source" and in the central part including the sedimentary basin. In addition, it is interesting to note that the station NM is located in the area with the lowest site effect potential, confirming thus the selection of this site as a reference station for the SSR computations.

5.3. Discussion of the Results with Respect to the General Tectonic Context and Outlining Elements for Sub-Regional Seismic Microzonation

We now discuss how the previous results fit in the geological and tectonic context, using as parameters the fundamental resonance frequency with its amplitude, the az-

imuth of the seismic wavefield, the shear wave velocity as well as the electrical resistivity. The computed fundamental resonance frequencies and amplitudes depict the existence of two resonant layers with variable thickness in most of the part of the sedimentary basin, particularly near its central axis. The two resonant layers in the basin are evidenced by the double peaks at respectively 2–4 Hz and 10–15 Hz. Such double frequency peaks have already been observed by Laurendeau et al. [49] in the basin of Quito in Ecuador. The latter interpreted the lower frequency peak as being related to the deeper impedance contrast and the more superficial one as being linked to shallow lacustrine deposits contrasting with harder deeper soils. Elsewhere in the sedimentary basin, single resonance peaks with frequencies ranging from 2 to 8 Hz and amplitudes higher than 2.5 are observed and site effects are therefore expected.

The absence of impedance contrast is demonstrated by the flat or almost flat spectral ratio curves found in wide areas on top of the alluvial fan. Initially, those results had not been expected as alluvial material often presents a high amplification potential. The relatively lower potential in the present case marked by the weak HVSR peak amplitudes can best be explained by larger compactness of the Plio-Quaternary deposits composing it so that their acoustic impedance is comparable to the one of the underlying bedrock.

Above it was outlined that the HVSR results in terms of resonance frequency and amplitude do not show any clear spatial tendency that could be related to a wider tectonic influence—resonance peak frequency and amplitude are thus more dependent on local variations of surface layer thickness and type of material. However, the azimuth of the HVSR peaks seems to hint at some tectonic influence on the E-W polarisation of the seismic wavefield, aligned with the main orientation of the EPG fault (see Figure 8), at least in the neighborhood of this structure (within a distance of less than 1–2 km), except for a small part on top of the alluvial fan. The parallelism between the fault strike and the polarization of the shaking hints also at trapping of the seismic waves within the rocks damaged and weakened by the tectonic activity and must thus be considered as an effect of the seismic ground motion amplification [50,51]—but to prove this effect, additional studies, including numerical modelling, are needed.

The distribution of shear wave velocity and electrical resistivity values also follows some larger spatial trend, similar to the one of the HVSR peak azimuth, but slightly offset to the North (see Figure 16), with the lower values concentrated along an E-W oriented zone in the central part of Fond Parisien (bound to the South by the EPGF structure) and the higher ones found in the southeastern corner and along the northwestern border of the investigated area. The higher values found in the southernmost part corroborate the assertion of the high density of the alluvial materials. The lower velocity and resistivity zone corresponds, in the western part of Fond Parisien, to a fractured area including the E-W Ganthier fold and, in the eastern part, to the basin of soft sediments where mostly double frequency peaks are found. This result suggests a crushing of the rocks by the folding in the western part. Assuming continuity of the folding activity eastward, and consequently, below the sedimentary basin, the aforementioned double peaks may be explained by a double impedance contrast between the shallow thin soils and the crushed rocks and between these latter and the deeper competent bedrock. Such assumption is in good agreement with the results by Cormier et al. [52] who could outline by performing seismic profiles in the Lake Azuei, such E-W trending folds below the lake. Such folds may be in connection with the western Ganthier fold. The folding, likely to be related also to the recent activity of EPGF (as the fold axis is sub-parallel to the fault strike), has deformed and weakened these layers.

The combined pattern of geophysical characteristics and tectonic context explains the sharp lateral contrast between the central part and the rest of Fond Parisien. This central zone, encompassing the area in the North of the village "La Source" that contains a sedimentary basin and some zones in the western part, is a weakened zone where strong local site effects could increase ground shaking during future earthquakes. Some topographic site amplification (related to small hills) may also contribute to local site effects in some central hilly parts (marked by HVSR peaks at around 1 Hz), particularly near the MN station site.

The site effects in Fond Parisien may thus be characterized as very complex, simultaneously involving combined effects of the neighborhood of EPGF, some topographic and (locally multi-) surface layer amplification and some more deeply rock-soils folded and weakened by tectonic stressing (possibly also intensely weathered and saturated).

6. Conclusions

In Haiti, during the January 2010 earthquake, several areas suffered from large damages related to site effects. These site effects were investigated at a regional scale for the whole agglomeration of Port-au-Prince [10,13]. More detailed studies were implemented by Hough et al. [11], Assimaki and Jeong [12] and more recently by Ulysse et al. [14,15] for a hilly area, Gros–Morne, located to the east of Port-au-Prince.

The present geophysical–seismological study of the local amplification potential (possibly combined in a few areas with a higher liquefaction potential, sensu Michetti et al. [53]) in Fond Parisien could demonstrate that site effects are higher in the central part where the lower shear wave velocities and resistivities were recorded (Figure 19). This zone in the North of the village "La Source" includes in its eastern part a small sedimentary basin, the shore of Lake Azuei, and coincides in its western part with the location of the Ganthier fold (possibly present also in the East under the sedimentary basin and even under the lake). The shear wave velocities in the soils of the sedimentary basin are very low to low (200 m/s–450 m/s). Very low resistivities (locally less than 20 Ωm) measured in this area indicate both a high water saturation and a high salinity of the water in these layers. Their fundamental resonance frequencies are very variable, 0.5 Hz to 7 Hz, with amplitudes ranging from 2 to 8. This variability observed in the frequency values points to a changing depth of the bedrock. The latter is deeper in the center and in some areas in the south of the basin as well as near the northern border of the alluvial fan. Moreover, most of the sites in the central part of the basin are marked by a double frequency peak, indicating the existence of two resonant soft layers overlying the competent basement.

The southeastern corner of Fond Parisien that is located on an alluvial fan is surprisingly marked by the weakest site effects and thus probably also by the lowest local seismic hazard (note, hazards related to floods or debris flows that are likely to affect the alluvial fan area have not been studied in the frame of the present project). An additional lower seismic hazard zone is located in the northwestern corner where soft rocks are found near the surface. Locally, also some topographical site effects were detected.
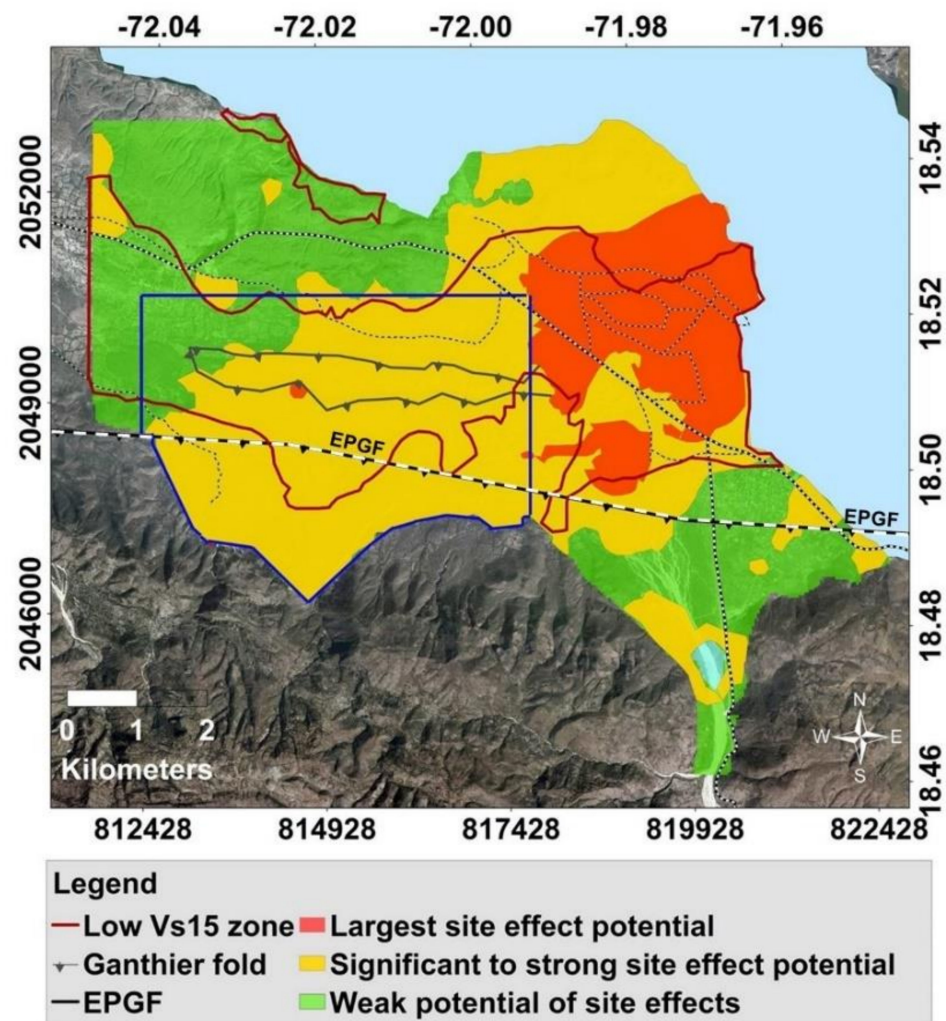
Figure 19. Map synthesizing the occurrence of the site effects across the Fond Parisien area. The zone with the largest potential of site effects, marked in red, is mostly located in the northern part of the sedimentary basin. Green shapes show the areas where the probability of the local ground shaking is weak or non-existent. The Ganthier fold is represented by the gray line. The black line shows the trace of the EPG Fault and the dark red line delimits the zones marked by low shear wave velocities.

Finally, the HVSR data, analyzed in terms of azimuth, evidenced a roughly E-W preferential directivity of the ambient noise wavefield, in the vicinity of the Enriquillo Plantain Garden Fault and in some scarce other places. This suggests a clear influence of the EPG Fault on the seismic wavefield orientation. However, this directivity could also be affected by some topographic features, as the southern part of Fond Parisien mostly presents surface irregularities. Further investigations should lead to determine how the fault and the topography individually contribute to the resulted main orientation of the seismic wavefield.

All these different elements potentially contributing to the sub-regional site effect distribution were synthesized in the map below. Indeed, the latter which is based on a qualitative classification of the site amplification potential shows the distribution of the site effects related to the subsurface layers and the location of the areas where topographical ground motion amplification is likely to occur together with the zones of the central part where the lower values of velocity and resistivity were found. This map can now be considered as a solid basis for a quantitative seismic microzonation project, in connection with possible future urbanization plans.
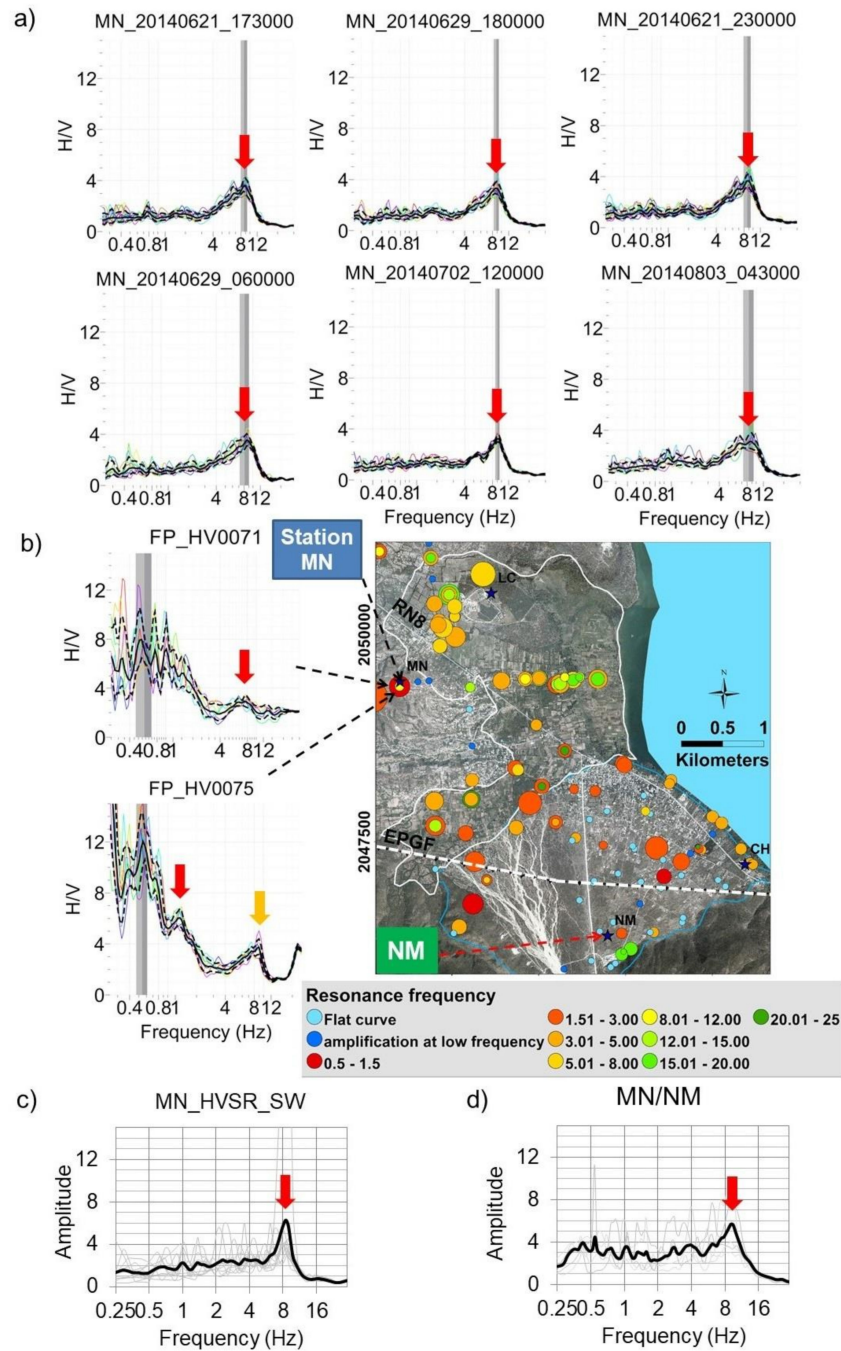
Appendix A

Figure A1. Spectral ratio curves computed for the MN site located near the western border for the sedimentary basin (the map, with white solid line delimiting the sedimentary basin, shows the HVSR results for that zone in terms of resonance frequencies and amplitude as colored circles of different sizes; see also Figure 7 for scales): (**a**) ambient noise HVSR curves for station MN records; (**b**) Tromino ambient noise HVSR curves; (**c**) and (**d**) respectively the earthquake HVSR and SSR curves (the latter using S-wave window spectra of NM station as reference). Red arrows indicate the fundamental resonance frequency; the orange arrow marks a second peak (at 8 Hz) in one Tromino ambient noise HVSR that corresponds to the fundamental peak on the other spectral ration curves.
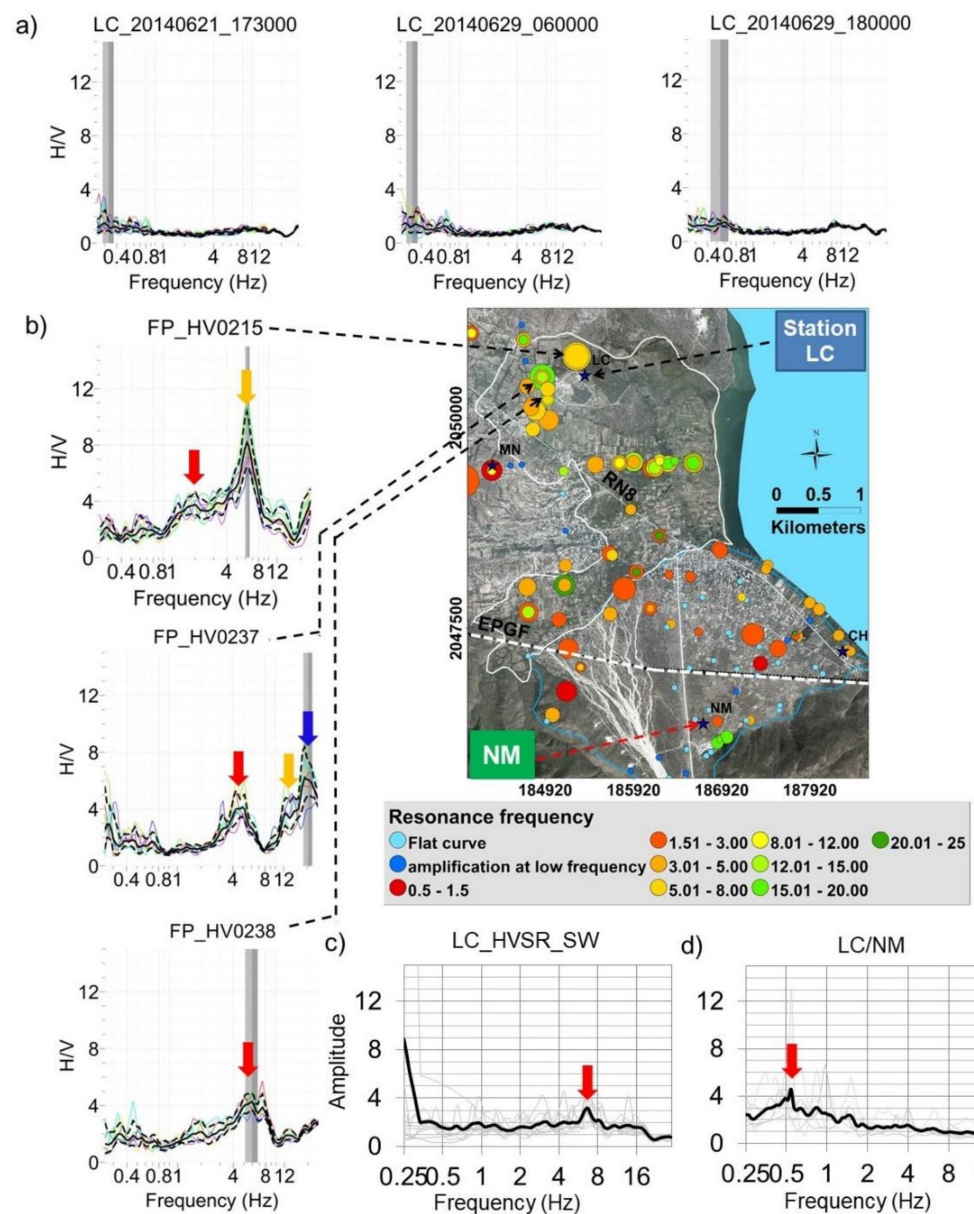
Figure A2. Spectral ratio curves computed for the LC site located in the northern part of the sedimentary basin (the map, with white solid line delimiting the sedimentary basin, shows the HVSR results for that zone in terms of resonance frequencies and amplitude as colored circles of different sizes; see also Figure 7 for scales): (**a**) ambient noise HVSR curves for station LC records; (**b**) Tromino ambient noise HVSR curves; (**c**) and (**d**) respectively the earthquake HVSR and SSR curves (the latter using S-wave window spectra of NM station as reference). Red arrows indicate the fundamental resonance frequency (both for Tromino ambient noise and LC station S-wave HVSR), yellow and blue arrows mark higher frequency peaks in Tromino ambient noise HVSR.

References

1. Daniell, J.; Khazai, B.; Wenzel, F.; Vervaeck, A. Damaging Earthquakes Database 2012: The Year in Review. *Nat. Hazards Earth Syst. Sci.* **2011**, *11*, 2235–2251. [CrossRef]
2. Bilham, R. Lessons from the Haiti earthquake. *Nat. Cell Biol.* **2010**, *463*, 878–879. [CrossRef]
3. Eberhard, M.O.; Baldridge, S.; Marshall, J.; Mooney, W.; Rix, G.J. *The MW 7.0 Haiti Earthquake of January 12, 2010: USGS/EERI Advance Reconnaissance Team Report*; US Geological Survey: Menlo Park, CA, USA, 2010.
4. Preptit, C. *Aléa et Risqué Sismique en Haiti*; Bureau des Mines et de l'Energie: Port-au-Prince, Haiti, 2008.
5. Flores, C.H.; Brink, U.S.T.; Bakun, W.H. *Accounts of Damage from Historical Earthquakes in the Northeastern Caribbean to Aid in the Determination of Their Location and Intensity Magnitudes*; US Geological Survey: Menlo Park, CA, USA, 2012.

6. Frankel, A.; Harmsen, S.; Mueller, C.; Calais, E.; Haase, J. *Documentation for Initial Seismic Hazard Maps for Haiti*; US Geological Survey: Menlo Park, CA, USA, 2010.
7. Frankel, A.; Harmsen, S.; Mueller, C.; Calais, E.; Haase, J. Seismic Hazard Maps for Haiti. *Earthq. Spectra* **2011**, *27*, 23–41. [CrossRef]
8. McNamara, D.; Meremonte, M.; Maharrey, J.Z.; Mildore, S.L.; Altidore, J.R.; Anglade, D.; Hough, S.E.; Given, D.; Benz, H.; Gee, L.; et al. Frequency-Dependent Seismic Attenuation within the Hispaniola Island Region of the Caribbean Sea. *Bull. Seism. Soc. Am.* **2012**, *102*, 773–782. [CrossRef]
9. Cox, B.R.; Bachhuber, J.; Rathje, E.; Wood, C.M.; Dulberg, R.; Kottke, A.; Green, R.A.; Olson, S.M. Shear Wave Velocity-and Geology-Based Seismic Microzonation of Port-au-Prince, Haiti. *Earthq. Spectra* **2011**, *27*, 67–92. [CrossRef]
10. Terrier, M.; Bialkowsky, A. *Microzonage Sismique de Port-au-Prince (Haiti): Etude Géologique*; Technical report. BRGM/RP-61243-FR, p.89, fig.48, ann.1; Bureau de recherche Géologique et Minière: Orléans, France, 2014.
11. Hough, S.E.; Altidor, J.R.; Anglade, D.; Given, D.; Janvier, M.G.; Maharrey, J.Z.; Meremonte, M.; Mildor, B.S.L.; Prepetit, C.; Yong, A.K. Localized damage caused by topographic amplification during the 2010 M 7.0 Haiti earthquake. *Nat. Geosci.* **2010**, *3*, 778–782. [CrossRef]
12. Assimaki, D.; Jeong, S. Ground-Motion Observations at Hotel Montana during the M 7.0 2010 Haiti Earthquake: Topography or Soil Amplification? *Bull. Seism. Soc. Am.* **2013**, *103*, 2577–2590. [CrossRef]
13. Fleur, S.S.; Bertrand, E.; Courboulex, F.; De Lépinay, B.M.; Deschamps, A.; Hough, S.; Cultrera, G.; Boisson, D.; Prépetit, C. Site Effects in Port-au-Prince (Haiti) from the Analysis of Spectral Ratio and Numerical Simulations. *Bull. Seism. Soc. Am.* **2016**, *106*, 1298–1315. [CrossRef]
14. Ulysse, S.; Boisson, D.; Prépetit, C.; Havenith, H.B. Site Effect Assessment of the Gros-Morne Hill Area in Port-au-Prince, Haiti, Part A: Geophysical-Seismological Survey Results. *Geoscience* **2018**, *8*, 142. [CrossRef]
15. Ulysse, S.; Boisson, D.; Prépetit, C.; Havenith, H.B. Site Effect Assessment of the Gros-Morne Hill Area in Port-au-Prince, Haiti, Part B: Mapping and Modelling Results. *Geoscience* **2018**, *8*, 233. [CrossRef]
16. Maurrasse, F.J.M.R. *Survey of the Geology of Haiti Guide to the Field Excursion in Haiti*; Miami Geological Society: Miami, FL, USA, 1982.
17. Meyerhoff, H.A. Section of Geology and Mireralogy: Antillean tectonics. *Trans. N. Y. Acad. Sci.* **1954**, *16*, 149–155. [CrossRef]
18. Butterlin, J. *Géologie Générale de la République d'Haïti. Travaux et Mémoires*; Institut des Hautes Études de l'Amérique Latine: Paris, France, 1960.
19. Momplaisir, R.; Boisson, D. *Carte Géologique de la République d'Haiti—Feuille Sud'Est*; Bureau of Mining and Energy: Port-au-Prince, Haiti, 1988.
20. Saint-Fleur, N. Sismotectonique du système de failles d'Enriquillo et du séisme du 12 janvier 2010 (Mw 7.0) en Haiti. Ph.D. Thesis, Institut du Globe de Physique de Paris—Université Paris Diderot, Paris, France, 2014.
21. Symithe, S.; Calais, E. Present-day shortening in Southern Haiti from GPS measurements and implications for seismic hazard. *Tectonophysics* **2016**, *679*, 117–124. [CrossRef]
22. Ministère de l'Agriculture des Ressources Naturelles et du Développement Rural. *Carte Hydrogéologique République d'Haïti*; Ministère de l'Agriculture des Ressources Naturelles et du Développement Rural: Port-au-Prince, Haiti, 1987.
23. Giocoli, A.; Stabile, T.A.; Adurno, I.; Perrone, A.; Gallipoli, M.R.; Gueguen, E.; Norelli, E.; Piscitelli, S. Geological and geophysical characterization of the southeastern side of the High Agri Valley (southern Apennines, Italy). *Nat. Hazards Earth Syst. Sci.* **2015**, *15*, 315–323. [CrossRef]
24. Nguyen, F.; Garambois, S.; Chardon, D.; Hermitte, D.; Bellier, O.; Jongmans, D. Subsurface electrical imaging of anisotropic formations affected by a slow active reverse fault, Provence, France. *J. Appl. Geophys.* **2007**, *62*, 338–353. [CrossRef]
25. Galli, P.A.C.; Giocoli, A.; Peronace, E.; Piscitelli, S.; Quadrio, B.; Bellanova, J. Integrated near surface geophysics across the active Mount Marzano Fault System (southern Italy): Seismogenic hints. *Acta Diabetol.* **2014**, *103*, 315–325. [CrossRef]
26. Park, C.B.; Miller, R.D.; Xia, J. Multichannel analysis of surface waves. *Geophysics* **1999**, *64*, 800–808. [CrossRef]
27. Foti, S.; Lai, C.G.; Rix, G.J.; Strobbia, C. *Surface Wave Methods for Near-Surface Site Characterization*; CRC Press: Hoboken, NJ, USA, 2014.
28. Strobbia, C. Surface Wave Methods Acquisition Processing and Inversion. Ph.D. Thesis, Politecnico Di Torino, Turin, Italy, 2003.
29. Renalier, F. Caractérisation Sismique de Sites Hétérogènes à Partir de Méthodes Actives et Passives: Variations Latérales et Temporelles. Ph.D. Thesis, University of Grenoble, Grenoble, France, 2006.
30. Mucciarelli, M.; Gallipoli, M.R.; Arcieri, M. The stability of the horizontal-to-vertical spectral ratio of triggered noise and earthquake recordings. *Bull. Seismol. Soc. Am.* **2003**, *93*, 1407–1412. [CrossRef]
31. Bonnefoy-Claudet, S.; Cornou, C.; Bard, P.-Y.; Cotton, F.; Moczo, P.; Kristek, J.; Fäh, D. H/V ratio: A tool for site effects evaluation. Results from 1-D noise simulations. *Geophys. J. Int.* **2006**, *167*, 827–837. [CrossRef]
32. Nakamura, Y.A. Method for dynamic characteristics estimation of subsurface using microtremor on the ground surface. *Railw. Tech. Res. Inst. Q. Rep.* **1989**, *30*, 25–33.
33. Lermo, J.; Chavez-Garcia, F.J. Are microtremors useful in site response evaluation? *Bull. Seismol. Soc. Am.* **1994**, *84*, 1350–1364.
34. Lachet, C.; Bard, P.Y. Numerical and Theoretical Investigations on the Possibilities and Limitations of Nakamura's Technique. *J. Phys. Earth* **1994**, *42*, 377–397. [CrossRef]
35. Nogoshi, M.; Igarashi, T. On the propagation characteristics of microtremor. *J. Seismol. Soc. Jpn.* **1971**, *23*, 264–280. [CrossRef]

36. Bard, P.; SESAME-Team. *Guidelines for the Implementation of the H/V Spectral Ratio Technique on Ambient Vibrations: Measurements, Processing, and Interpretations*; SESAME European Research Project Report WP12–Deliverable D23.12, European Commission–Research General Directorate Project No. EVG1-CT-2000-00026 SESAME; Springer: Berlin, Germany, 2004.

37. Ibs-von Seht, M.; Wohlenberg, J. Microtremor measurements used to map thickness of soft sediments. *Bull. Seism. Soc. Am.* **1999**, *89*, 250–259. [CrossRef]

38. Borcherdt, R.D. Effects of local geological geology on ground motion near the San Francisco. *Bull. Seismol. Soc. Am.* **1970**, *60*, 29–61.

39. Borcherdt, R.D.; Gibbs, J.F. Effects of local geological conditions in the San Francisco bay on ground motions and the intensities of the 1906 earthquake. *Bull. Seismol. Soc. Am.* **1976**, *66*, 467–500.

40. Layadi, K.; Semmane, F.; Yelles-Chaouche, A.K. Site-Effects Investigation in the City of Chlef (Formerly El-Asnam), Algeria, Using Earthquake and Ambient Vibration Data. *Bull. Seism. Soc. Am.* **2016**, *106*, 2185–2196. [CrossRef]

41. Michel, C.; Hannewald, P.; Lestuzzi, P.; Fäh, D.; Husen, S. Probabilistic mechanics-based loss scenarios for school buildings in Basel (Switzerland). *Bull. Earthq. Eng.* **2017**, *15*, 1471–1496. [CrossRef]

42. Loke, M.H. Tutorial: 2-D and 3-D Electrical Imaging Survey. 2001. Available online: https://pangea.stanford.edu/research/groups/sfmf/docs/DCResistivity_Notes.pdf (accessed on 25 January 2021).

43. Wathelet, M. *GEOPSY Geophysical Signal. Database for Noise Array Processing. Software 2005*; LGIT: Grenoble, France, 2005.

44. Konno, K.; Ohmachi, T. Ground-Motion Characteristics Estimated from Spectral Ratio between Horizontal and Vertical Components of Microtremor. *Bull. Seismol. Soc. Am.* **1998**, *88*, 228–241.

45. Pischiutta, M.; Fondriest, M.; Demurtas, M.; Magnoni, F.; Di Toron, G.; Rovelli, A. Structural control on the directional amplification of seismic noise (campo imperatore, central Italy). *Earth Planet. Sci. Lett.* **2017**, *471*, 10–18. [CrossRef]

46. Burjanek, J.; Fäh, D.; Pischiuttan, M.; Rovelli, A.; Calderonin, G.; Bard, P.Y.; NERA-JRA1 Working Group. *Site Effects at Sites with Pronounced Topography: Overview and Recommendations. Research letter for EU project NERA*; Technical report 2014; ETH-Zürich: Zürich, Switzerland, 2014; p. 64. [CrossRef]

47. Havenith, H.B.; Torgoev, I.; Ischuk, A. Integrated Geophysical-Geological 3D Model of the Right-Bank Slope Downstream from the Rogun Dam Construction Site, Tajikistan. *Int. J. Geophys.* **2018**, *2018*, 1–16. [CrossRef]

48. Johnson, M.W.; Chittenden, R.N.; Crouse, C.B.; Hawkins, N.M.; Kelly, D.J.; Power, M.S.; Wey, E.H. *Minimum Design Loads for Buildings and Other Structures*; American Society of Civil Engineers: Reston, VA, USA, 2010.

49. Laurendeau, A.; Courboulex, F.; Bonilla, L.F.; Alvarado, A.; Naya, V.A.; Guéguen, P.; Mercerat, E.D.; Singaucho, J.C.; Bertrand, E.; Perrault, M.; et al. Low-Frequency Seismic Amplification in the Quito Basin (Ecuador) Revealed by Accelerometric Recordings of the RENAC Network. *Bull. Seism. Soc. Am.* **2017**, *107*, 2917–2926. [CrossRef]

50. Wu, J. New Constraints on Fault-Zone Structure from Seismic Guided Waves. Ph.D. Thesis, Virginia Polytechnic Institute and State University, Blacksburg, VA, USA, 2008.

51. Di Giulio, G.; Cara, F.; Rovelli, A.; Lombardo, G.; Rigano, R. Evidences for strong directional resonances in intensely deformed zones of the Pernicana fault, Mount Etna, Italy. *J. Geophys. Res. Space Phys.* **2009**, *114*. [CrossRef]

52. Cormier, M.H.; Sloan, H.; Boisson, D.; Brown, B.; Guerrier, K.; Hearn, C.K.; Heil, C.W.; Kelly, R.P.; King, J.W.; Stampel, R.; et al. *Signature of Transpressional Tectonics in the Holocene Stratigraphy of Lake Azuei, Haiti: Preliminary Results from a High-Resolution Subbottom Profiling Survey*; American Geophysical Union: Washington, DC, USA, 2017.

53. Michetti, A.M.; Esposito, E.; Guerrieri, L.; Porfido, S. Environmental Seismic Intensity Scale—ESI 2007. *Mem. Descr. Carta Geol. Italia* **2007**, *74*, 7–54.